NP-14544

QUARTERLY TECHNICAL SUMMARY REPORT

ON

DIRECT ENERGY CONVERSION SYSTEMS

Supplement 1

HEAT AND MASS TRANSFER FROM THE SURFACE OF A
CYLINDER WITH DISCONTINUOUS BOUNDARY
CONDITIONS TO AN INCOMPRESSIBLE LAMINAR FLOW

Prepared for

Advanced Research Projects Agency

Submitted by

Robert H. Eustis, Principal Investigator

Written by

Zeev Rotem and David M. Mason

For the period

1 June 1964 - 31 August 1964

ARPA Order Number:	246, Amendment 6
Program Code Number:	3980
Name of Contractor:	Board of Trustees of the Leland Stanford Junior University
Date of Contract:	1 November 1961
Contract Number	AF 49(638)-1123
Contract Expiration Date:	31 August 1964

September 30, 1964

Stanford, California

STANFORD UNIVERSITY ■ STANFORD, CALIFORNIA

ABSTRACT

Heat and mass transfer studies for flow over a cylinder having a longitudinal-strip source of heat or mass, are presented. A theory for the two asymptotic cases of $Pr \to \infty$ and $Pr \to 0$ is developed, giving the temperature profile and the transfer rate for such a strip. The theory includes the effect of the conductivity of the heating strip material. It is shown that if the conductivity of the strip material is very high, then the transfer rate is a measure of local wall shear-stress provided the Prandtl number of the convecting fluid is high.

Experimental studies described include electrochemical mass-transfer studies carried out on a rotating cylindrical electrode carrier; and heat transfer studies carried out in an oil tunnel. Fair correlation between theory and experiment was found.

TABLE OF CONTENTS

LIST OF FIGURES

LIST OF TABLES

LIST OF SYMBOLS

A	interfacial area
$\mathcal{A}$	function of X, see eq. (2.9)
b	width
Bi	Biot modulus = $H\ell/K_{solid}$
c	concentration
c_f	friction factor = $\tau/(\rho U^2)$
C	constant
$\mathfrak{D}$	diffusion coefficient
f	frequency; function
F	Faraday constant
g	acceleration of gravity
Gr	Grasshoff modulus = $\dfrac{g\ell^3 \Delta\rho}{\nu^2 \rho}$
H	heat transfer coefficient; also mass transfer coefficient
i	index
I	electrical current
i'	electrical current density
K	thermal conductivity
ℓ	characteristic length
L	axial length of cylinder
m	index
M	reduced heat source strength
n	index

Nu	Nusselt modulus = $q'' \ell / (K \cdot \theta_s)$
N_ν	chemical valence
P_1	dimensional pressure
p	dimensionless pressure in terms of 2 velocity heads
Pe	Peclet modulus = $U\ell / \kappa$
Pr	Prandtl modulus = ν / κ
q''	heat flux
q_s'''	heat, source strength
r	radius, Appendix II
R	radius
Re	Reynolds modulus = $\rho U \ell / \mu$
s	index
S	Strouhal modulus = $f\ell / U\infty$
Sc	Schmidt modulus = $\nu / \mathcal{D}$
Sh	Sherwood modulus = $H\ell / \mathcal{D}$ (mass transfer)
$T, \hat{T}$	reduced dimensionless temperature
TR	transfer rate
u, v, w	velocity vector components
u_1, v	dimensional velocity components
U	outer flow velocity
V	$v \cdot Re^{1/2}$; also voltage (Appendix II)
x, y, z	dimensionless cartesian axes of coördinates
x_1	dimensionless coördinate; in (3.7) and Appendix II: dimensional abscissa
$\hat{x}$	"stretched" dimensionless coördinate

y_i	dimensional ordinate
x^*	smallest abscissa for which $\theta \neq 0$
X	dimensionle coördinate (Appendix II)
Y	$y \cdot Re^{1/2}$

β	dimensionless shear stress at the wall $= c_f \sqrt{Re}$
γ	function of x, ($\S$ 2.1-2)
Γ	gamma function
o	thickness
	difference; also angular extent of strip in x direction
$\Delta\rho$	density change taking place at interface
ϵ	small parameter
ζ	dummy variable
η	dummy variable
ϑ	dimensionless temperature difference
θ	temperature difference; also, dimensionless temperature differen
κ	thermal diffusivity
Λ	generalized function
μ	dynamic viscosity
ν	function of x ($\S$ 2.2-1); kinematic viscosity
π	in Appendix I; dimensionless pressure
ρ	density
ρe	electrical resistivity
τ	shear stress

φ angle

Abbreviations

FSP   Front stagnation point

RSP   Rear stagnation point

TR   Transfer rate

Subscripts

o, s   refer to surface (except in Appendix II where s refers to source)

∞ refers to outer flow

1. Introduction

The purpose of the present report is the presentation of both theoretical and experimental results for the transfer of heat and mass from or to a long circular cylinder immersed in a two-dimensional flow of an incompressible, isotropic, Newtonian fluid. The flow is of laminar boundary layer type, with a step type heat (or mass) flux source on the cylinder envelope.

The subject of heat transfer in external flow has been studied previously by a large number of investigators, both theoretically [1-7] and experimentally [8, 9] *. In particular, asymptotic solutions for the cases of extremely large and extremely small Prandtl or Schmidt moduli, and for many kinds of temperature boundary conditions at the cylinder surface have been known for some time [7]. Now, hese analytical solutions depend upon the detailed knowledge of the external flow around the cylinder as a function of coördinate. This information is obtainable either from the analysis of an assumed idealized flow field (see c.f. [10]), at least up to that value of the coördinate in the flow direction where boundary layer separation takes place; or else it has to be obtained from a semi-empirical approach which takes into account actual test conditions (see c.f. [13, 14]). However, beyond the point of boundary layer separation little is known about wall shear-stress values and local heat and mass transfer rates.

There has recently been some interest in the reinvestigation of two dimensional, incompressible, laminar, steady and separated flow behind bluff objects [14, 15]. This problem is both of obvious practical significance in the estimation of the drag of such bodies, and of fundamental theoretical importance in the investigation of the stability of two dimensional flows and the uniqueness of the flow field at (comparatively) high values of the Reynolds number. The choice of suitable flow models to represent such separated flows must perforce depend on at least some rudimentary knowledge of the flow conditions inside the region of separation (the wake bubble).

---

*For a summary of previous work see c.f. [10, 11] and [12].

The present report will describe a mass and heat transfer experiment in which the flux source (or sink) is a narrow strip bounded by two generating lines on the cylinder envelope. It will be shown that, provided this strip is sufficiently narrow, the transfer rate from its surface depends only on the local wall shear stress. Thus the measurement of the transfer rate may be translated immediately into a local wall shear stress, information probably not obtainable from any other simple experiment.

The design of the experimental apparatus will be described, and experimental results will be compared with theoretical predictions.

2. Theory

It will be found useful to review here briefly Lighthill's [3] asymptotic solution for the heat (or mass) transfer to laminar boundary layer flows at very high and very low values of the Prandtl modulus (respectively the Schmidt modulus in the case of mass transfer).

We shall introduce the boundary layer approximations into the dimensionless equations of momentum, continuity and energy for the flow of an incompressible, non-dissipative, isotropic, Newtonian, constant physical property fluid to obtain,

$$u \frac{\partial u}{\partial x} + V \frac{\partial u}{\partial Y} = - \frac{\partial p}{\partial x} + \frac{\partial^2 u}{\partial Y^2}$$

$$\frac{\partial u}{\partial x} + \frac{\partial V}{\partial Y} = 0 \qquad \qquad \Bigg\} \qquad \ldots(2.1)^{(*)}$$

$$u \frac{\partial \theta}{\partial x} + V \frac{\partial \theta}{\partial Y} = \frac{1}{Pr} \frac{\partial^2 \theta}{\partial Y^2}$$

with boundary conditions,

$$
\begin{aligned}
x &< x^*; & \theta &= 0; \\
x &\geq 0; \quad Y = 0; & u &= V = 0; \\
& Y = \infty; & \theta &= 0; \quad u = U(x); \\
x &\geq x^*; \quad Y = 0; & \theta &= \theta(x);^{(**)}
\end{aligned}
\Bigg\} \qquad \ldots(2.2)
$$

In what follows interfacial velocities will be neglected so that the equations above will be applicable to both the transfer of heat and mass. For the latter case the Sherwood number is to be read whenever the Nusselt number appears, and the Schmidt number for the Prandtl number.

2.1 Large Prandtl or Schmid moduli

For $Pr \gg 1$ the thermal boundary layer may be assumed to be very thin in comparison with the momentum boundary layer. $u(x, Y)$, being an analytic function within the flow field, may thus be expanded in a Taylor series around its value on

---

(*) see list for explanation of symbols
(**) respectively $\partial \theta / \partial y$ prescribed.

the boundary. Following Lévêque [16] only the first term of the expansion will be retained (see Appendix I). Then a solution of equations (2.1) satisfying (2.2) is found to be (see c.f. [7]),

$$\theta = \frac{1}{\Gamma(\frac{4}{3})} \int_{\eta}^{\infty} e^{-\eta^3} \, d\eta$$

$$-\frac{\partial\theta}{\partial y}\bigg|_{y=0} = Nu = \frac{Re^{\frac{1}{2}} Pr^{\frac{1}{3}}}{9^{\frac{1}{3}}\Gamma(\frac{4}{3})} \sqrt{\beta(x)} \int_{0}^{x} \frac{d\theta_s(x)}{\left[\int_{x^*}^{x}\sqrt{\beta(\zeta)}\,d\zeta\right]^{\frac{1}{3}}} \qquad \ldots(2.3)$$

Here x* is the dimensionless abscissa of the first point of non-zero θ_s

Several subcases representing idealized situations may now be considered:

2.1-1 Interface temperature (or concentration in the case of mass transfer) zero for x < x*, and equal to a non-zero constant for x ≥ x*.

For this case the second of equations (2.3) reduces to,

$$Nu = \frac{Re^{\frac{1}{2}} Pr^{\frac{1}{3}}}{9^{\frac{1}{3}}\Gamma(\frac{4}{3})} \cdot \frac{\sqrt{\beta(x)}}{\left[\int_{x^*}^{x}\sqrt{\beta(\zeta)}\,d\zeta\right]^{\frac{1}{3}}} \qquad \ldots(2.4)$$

To get the average value of the Nusselt modulus in two dimensional flow over a heating surface extending from x* to x, we may integrate equation (2.4):

$$\bar{Nu} = \frac{3^{\frac{1}{3}}}{2\cdot\Gamma(\frac{4}{3})}\cdot Re^{\frac{1}{2}} Pr^{\frac{1}{3}} \frac{\left[\int_{x^*}^{x}\sqrt{\beta(\zeta)}\,d\zeta\right]^{\frac{2}{3}}}{x - x^*} \qquad \ldots(2.5)$$

If the heated surface is relatively narrow in the x-direction, then $\sqrt{\beta(\zeta)}$ may be assumed to be essentially constant from x* to x; the equation above then simplifies to -

$$\bar{Nu} = \frac{Re^{\frac{1}{2}}}{2\cdot\Gamma(\frac{4}{3})}\left[\frac{3 Pr \bar{\beta}(\zeta)}{x - x^*}\right]^{\frac{1}{3}} \qquad \ldots(2.6)$$

where $\bar{\beta}$ is some average value of $\beta(\zeta)$:

$$\bar{\beta}(\zeta) = \left[\frac{\int_{x}^{x^*}\sqrt{\beta(\zeta)}\,d\zeta}{x - x^*}\right]^{2} \qquad \ldots(2.6-a)$$

It is apparent from equation (2.6) that the measurement of the surface temperature of a strip of suitable dimensions and the calculation of the average dimensionless flux will furnish directly an amplified value of the local shear stress at the wall, quite independently of previous boundary layer history.

2.1-2 <u>Zero interface heat flux for $x < x^*$, non-zero interface flux for $x \geq x^*$.</u>

We shall investigate the case in which the surface flux changes in steps of finite size; cases of continuous flux variation are easily derived from these results by superposition and passage to the limit. Define,

$$\Lambda_i (x_1) = q_i'' \; \frac{\ell}{K} \cdot \frac{Pr \quad Re}{3^{1/\cdot}\cdot\Gamma\left(\frac{}{3}\right)} \quad (i = 0, \; 1, 2, \ldots \ldots n) \qquad \ldots (2.7)$$

where q_i'' is a surface heat density increment; l is a characteristic length and x_1 is the coördinate location considered. Then,

$$\theta_s (x_1) = \Lambda_0(x_1) + \left[\Lambda_1(x^*) - \Lambda_0\right] \mathcal{H}(x_1 - x^*) +$$

$$+ \left[\Lambda_2(x^{**}) - \Lambda_1(x^*)\right] \mathcal{H} (x_1 - x^{**}) + \ldots$$

$$= \Lambda_0 \mathcal{H}(x_1) + \sum_{m=1}^{n} \left(x_1 - x^{(m*)}\right) \left(\frac{\Delta \Lambda}{\Delta x^*}\right)_{(m*)} \Delta x^* \qquad \ldots (2.8)$$

Here the Λ_i are the step magnitudes, occurring at abscissae x^{i*}, and -

$$\mathcal{H}(x_1) = \int_0^{x_1} \frac{dx}{\left[\gamma(x_1) - \gamma(x)\right]^{2/3}} \qquad \ldots (2.9)$$

$$\gamma(x) = \int_0^{x_1} \sqrt{\beta(\zeta)} \; d\zeta \qquad \ldots (2.10)$$

Specializing for a single step, we get Shah's expression ([17], p. 60):

$$\theta_s (x_1) = q_i'' \; \frac{\ell}{K} \; \frac{Pr^{-1/3} Re^{-1/2}}{3^{1/3}\Gamma\left(\frac{-}{3}\right)} \int_{x^*}^{x_1} \frac{dx}{\left[\gamma(x_1) - \gamma(x)\right]^{1/3}} \qquad \ldots (2.11)$$

Also,

$$Nu = \frac{q_i''\ell}{\theta_s K}$$

$$= 3^{1/3}\Gamma\left(\frac{2}{3}\right) Pr^{1/3} Re^{1/2} \left\{\int_{x^*}^{x_1} \frac{dx}{\left[\gamma(x_1) - \gamma(x)\right]^{1/3}}\right\}^{-1} \qquad \ldots (2.12)$$

for the single step-type flux variation at the wall.

The equivalent mean surface temperature and the mean Nusselt number over a strip of small finite width in the direction of flow, bounded by two parallel cylinder generating lines, may now be calculated. Proceeding in a manner analogous to § 2.1-1 and assuming $\sqrt{\beta(\zeta)}$ constant over the strip width one obtains,

$$\bar{\theta}_s = \frac{q_i''\ell}{K} \frac{2}{\Gamma(\frac{2}{3})} \left(\frac{x_1 - x^*}{3\bar{\beta}\, Pr} \right)^{1/3} Re^{-1/2} \qquad \ldots (2.13)$$

and

$$\bar{Nu} = \frac{1}{2}\Gamma\left(\frac{2}{3}\right) \left[\frac{3\bar{\beta}\, Pr}{x_1 - x^*} \right]^{1/3} Re^{1/2} \qquad \ldots (2.14)$$

2.1-3 **Cases departing from the idealized situations of piecewise constant interface temperature (respectively concentration) or flux**

In actual practice none of the idealized situations analyzed in the preceding paragraphs is ever attained. Usually an interface wall containing distributed heat sources, or their equivalent, over part of its length is convection cooled by some fluid. In general the distribution of these heat sources will not correspond to the rates of convection to the cooling fluid: indeed, only one unique distribution could be thus compatible. Consequently some circumferential conduction (i.e. conduction parallel to the direction of fluid flow) will ensue. If the resistance of the wall material containing the heat sources to the conduction of heat is slight, then the interface may be expected to approach an isothermal surface. If however that resistance should be very large, then the interface flux rate will correspond to the local wall flux density, and we approximate case 2.1-2. By small and large resistances to the conduction of heat within the wall material are here meant small and large values of the Biot modulus respectively (see Appendix II).

It will be shown in Appendix II that the temperature distribution for the case of an almost isothermal wall is easily derived through a regular perturbation scheme, while that of the almost constant flux case may be solved through a singular perturbation method, at least in principle.

2.2 **Small Prandtl or Schmidt moduli**

For $Pr \ll 1$ the momentum boundary layer will be rather thin compared to the thermal boundary layer. Thus the momentum boundary layer may be disregarded entirely in the solution of the energy equation and the velocity will be a function of the lengthwise coördinate only. Appropriate asymptotic solutions may then easily be obtained.

2.2-1 Interface temperature zero for $x < x^*$ and equal to a non-zero constant for $x \geq x^*$

$$Nu = \left[\frac{Pe}{\pi} \frac{(U(x))^2}{\int_{x^*}^{x} U(x)\,dx} \right]^{1/2} \qquad \ldots (2.15)$$

Whence the average value of Nu over a strip width $x_1 - x^*$ is obtained,

$$\bar{Nu} = 2 \left[\frac{Pe}{\pi} \int_{x^*}^{x} U(x)\,dx \right]^{1/2} \qquad \ldots (2.16)$$

2.2-2 Zero interface flux for $x < x^*$; non-zero, constant flux for $x \geq x^*$

The methods described in the previous paragraphs may again be used. Thus,

$$Nu = \Gamma\left(\tfrac{1}{2}\right) \sqrt{\frac{Pe}{\pi}} \left\{ \int_{x^*}^{x_1} \frac{dx}{[\mathcal{V}(x_1) - \mathcal{V}(x)]^{1/2}} \right\}^{-1} \qquad \ldots (2.17)$$

with -

$$\mathcal{V}(x) = \int_0^x U(\zeta)\,d\zeta$$

We may again assume a mean, constant outer-flow velocity to be operative over the strip width; then,

$$\bar{Nu} = \sqrt{\frac{U\,Pe}{\pi}} \; \frac{\Gamma\left(\tfrac{1}{2}\right)}{2} (x_1 - x^*)^{-1/2} \qquad \ldots (2.18)$$

and,

$$\bar{\theta} = \left(\frac{\pi}{U\,Pe} \right)^{1/2} \frac{q''\ell}{K} \cdot \frac{2}{\Gamma\left(\tfrac{1}{2}\right)} \sqrt{x_1 - x^*} \qquad \ldots (2.19)$$

The further extension to a prescribed, stepwise variation in wall flux rates is carried out without difficulty, and will therefore not be elaborated upon here.

3. Experimental: Mass Transfer Studies

3.1 Introduction

An initial survey of the relevant literature showed that the little work which had been done on local mass transfer rates from cylinders in forced convection at low Reynolds numbers (Schnautz 1958, Grassmann et al. 1961) was concerned with constant interface concentration over the entire cylinder envelope. It was also found that of the various techniques available for mass transfer studies, an

electrochemical methods appeared to be the most suitable. According to previous studies ([19] to [21]) such systems should have been capable of yielding results of great accuracy and good reproducibility with a comparatively simple experimental arrangement and without elaborate instrumentation. Consequently this was the first experimental system chosen for investigation.

3.2 Electrochemical details

By choosing a suitable electrochemical system, in which electron transfer at a test electrode surface is proceeding at a very high rate, it is possible to obtain a range of E. M. F. over which the transfer rate, i.e. the current measured, is independent of the driving force (the E. M. F.) applied. The transfer rate will depend only on the characteristics of the chemicals involved, of the surface at which transfer takes place and on the rate of supply of ions through the mass transfer boundary layer, that is on the convection rate. The current measured in this range is known as the limiting current.

Electrochemical systems which may be successfully used in this way must possess the following characteristics: (a) the active, transported chemical should have a very fast reaction rate at the active electrode surface; (b) the active chemical should be reasonably stable so that no noticeable changes in concentration occur while the experiment proceeds; (c) a supporting electrolyte should be present in a concentration sufficient to eliminate electrostatic field effects in the bulk fluid, and such that the polarization resistance at the ι surface is always the controlling factor; (d) the rate of any other electron transfer reactions taking place must be sufficiently slow so as not to affect the primary reaction rates studied.

Reliable quality gauges of an electrochemical test system are supplied by the following: (a) the "residual current", measured with the experimental electrochemical apparatus under test conditions, however with the active species in the solution missing, is a measure of the rate of extraneous, unwanted reactions taking place concurrently with the rate which is to be monitored. This residual current may be reduced to very low values through the use of clean solvent and chemicals, and the protection of the solution from the absorption of atmospheric oxygen and from incident light when necessary; (b) the functional dependence of the current on the E. M. F. applied will enable a conclusion to be reached as to the suitability of the system and the activity of the exchange surface. When the current measured (with

the electrode at rest, or at any one, steady speed) is plotted versus the voltage
the limiting current should indeed be constant over a substantial range of E. M. F.
(of the order of one volt). The level of this current "plateau" should be unaffected
by cycling. A deterioration in reproducibility of the polarograph and a "sluggishness"
in attaining a stationary value of the current when convective flow or voltage are
changed may be an indication of surface unsuitability or poisoning. Most surfaces
appear to deteriorate after a period of operation: this phenomenon does not appear
to be well understood.

The first system to be chosen for study was the reduction of oxygen on a
metallic gold surface in a (nominally) neutral solution, with KCl (or $KClO_4$) as
a supporting electrolyte. This system was reputed to have worked satisfactorily
before (Dr. P. Stonehart): nevertheless no proper limiting current plateau could
be obtained with the test system here described, and reproducibility of data was
generally poor. It has the added disadvantage that, with the method of oxygen
saturation recommended for this case by the electrochemists (simply bubbling air
through the solvent) no reliable value for oxygen concentration could ever be ob-
tained, while at the same time the solution must have contained appreciable amounts
of contaminant gases.

Later a more classical redox system. $Fe(CN)_6^{3-} \rightleftharpoons Fe(CN)_6^{4-}$ was used.
This system has been well documented in the relevant literature and property values
are well known. Tests were performed with several concentrations of active
ions   , and with different supporting electrolytes: for all test series up to and
including XI both the trivalent and the tetravalent salts in 1/100 normal concentra-
tion each were used (Vielstich, [22]; Stonehart), with KCl excess: for test series
XII and XIII the concentration of the hexacyanoferrates was increased to 5/100
equivalent per litre, to reduce the importance of any stray reactions and residual
currents (Dr. N. Ibl, [23]), in excess NaOH. lastly. in test series XIV only the
ferri salt was used, as all tests were performed with the exchange surface electro-
negative. This last composition of the solution seemed to lead to the best repro-
ducibility of results.

3.3 Experimental rig

3.3-1 General

Figure (1) shows the experimental equipment schematically; figure (2) is an

SPEED REDUCER
TRAILING WIRE

HG REFERENCE ELECTRODE

DRIVE

VOLTS (+)

(+)

SEAL
VIBRATION DAMPING
GLASS CONTAINER
STAYS
TEST ELECTRODE CARRIER
LEVELLING SHIMS

PERSPEX COVER
THERMOMETER
REF. ELECTRODE CARRIER
SINTERED GLASS FILTERS

COUNTER ELECTRODE
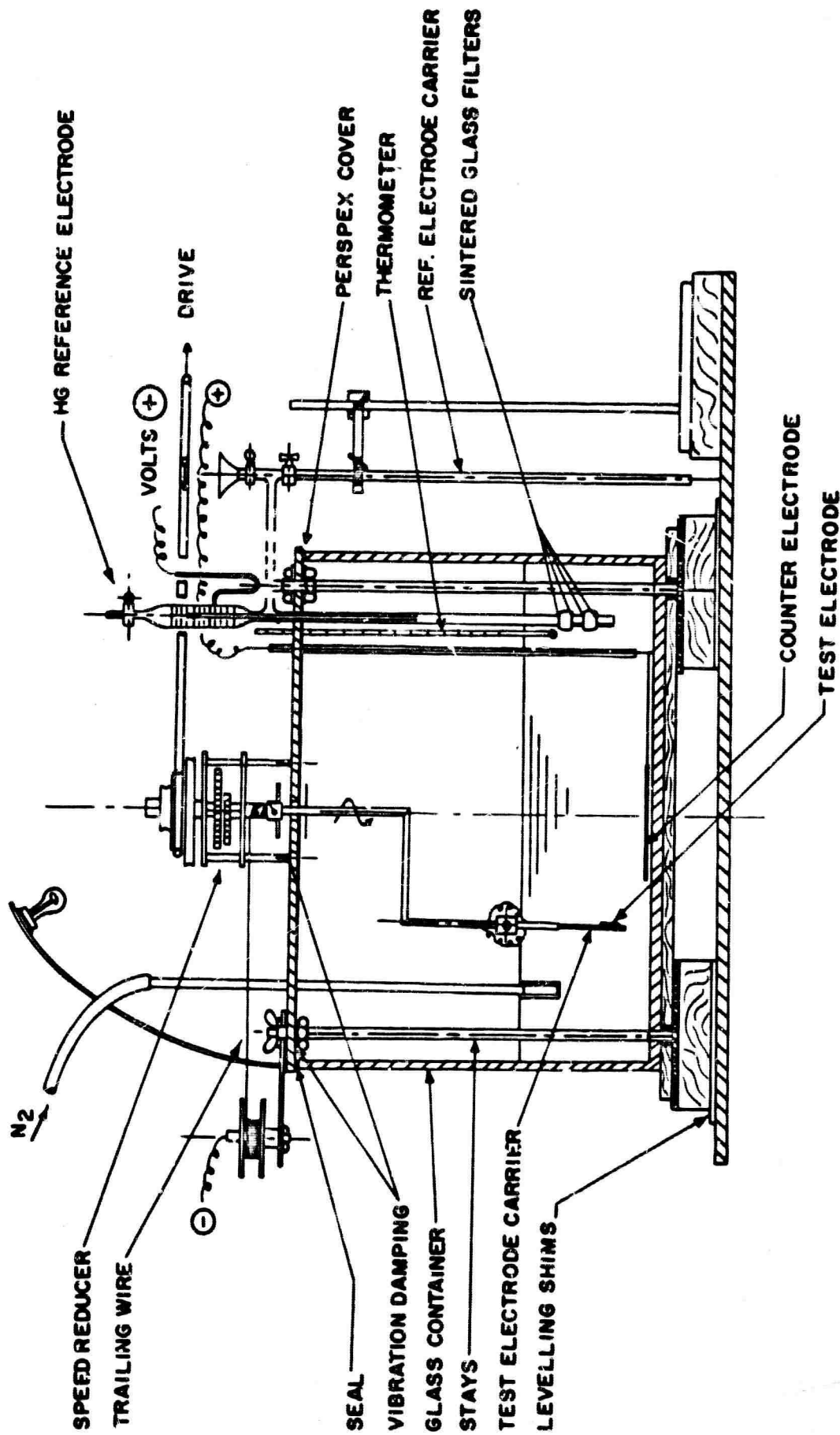TEST ELECTRODE

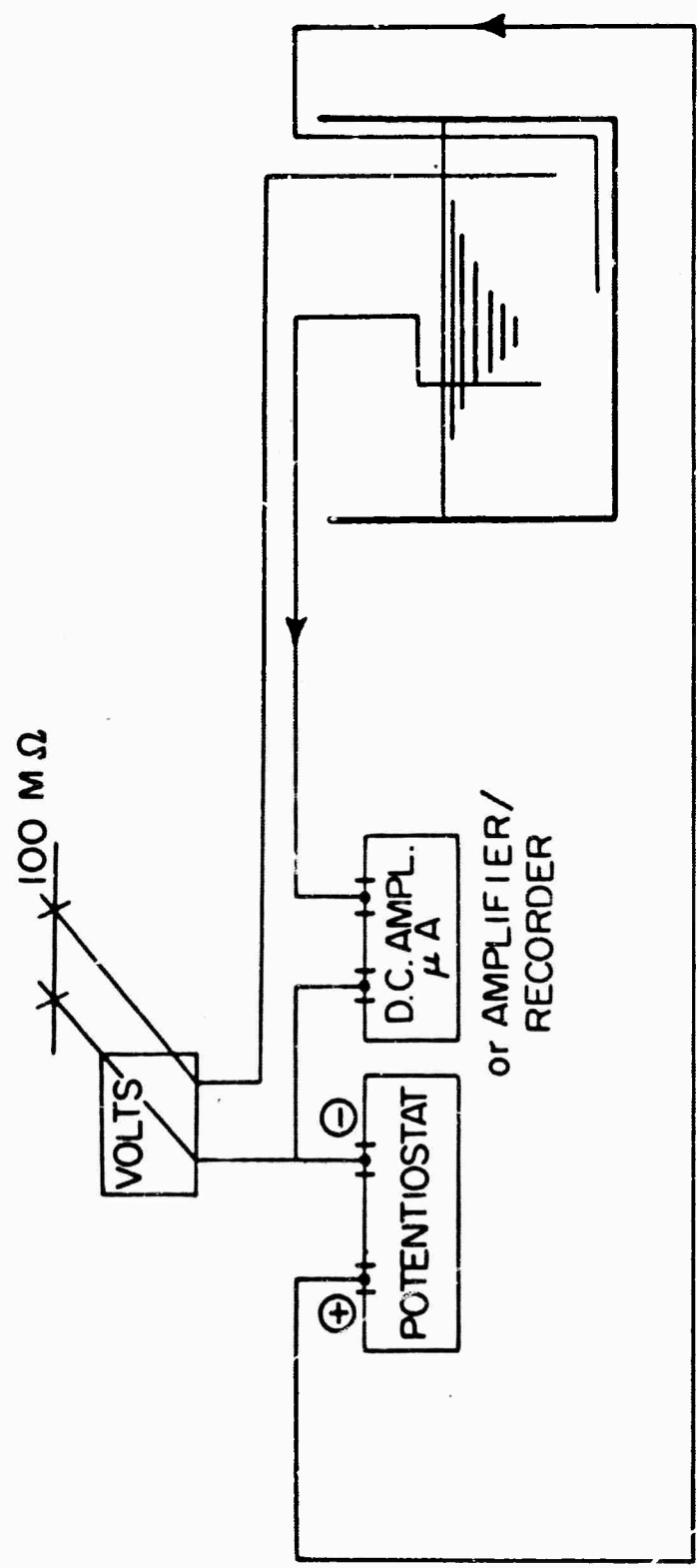N₂

(−)

FIGURE I.   SCHEMATIC DRAWING OF TEST APPARATUS.

FIGURE 2. DIAGRAM OF ELECTRICAL CONNECTIONS.

electrical circuit diagram while the plate, figure (3), shows the assembled equipment.

The apparatus ...sists essentially of a cylindrical vessel of soda lime glass 17-1/2 inches in diameter and 18 inches deep. A "Perspex" cover carries a drive mechanism to which a rotating arm assembly is attached. A cylindrical electrode carrier of 1/8 to 1/4 inch diameter is mounted on the rotating arm, and the latter is driven in a circular motion by the drive mechanism. Thus the test electrode moves along the circumference of a circle of about 4.62 inches radius. The glass container is filled with electrolytic fluid to a height of about 5-3/4 inches.

A constant voltage transformer supplies an induction motor which in turn drives the rotating arm assembly through assorted step-down devices.

The D.C. to the test bath is supplied from a potentiostat: the test surface is usually acting as the cathode. The anode is a platinum foil "counterelectrode". Current is taken off through a trailing wire connected to the test electrode. This method of current take-off was chosen for its simplicity over the more elegant and orthodox mercury pool slipring or sintered carbon brushes: thus also the number of items requiring development was reduced by one.

Much time was spent on insuring that both the test vessel and its cover were mounted horizontally. To reduce free surface* effects the active test e' ctrode area extended only a comparatively short vertical distance, deep inside the body of the fluid. Finally, to insure a steady rate of rotation of the electrode carrier the driving motor used was of ample size, and the final step down pinion was mounted on ball bearings. Anti-vibration mounting was used throughout.

During initial tests at very low transfer rates and speeds it was found that stray vibration and cantilever bending resonance of the test electrode carrier were on occasion increasing transfer rates notably. It took much effort to eliminate these secondary effects, but the phenomenon pointed towards the potential usefulness of the experimental method for the measurement of instationary mass transfer processes. In this respect the present technique has the advantage over heat transfer measurements in that, when used with a fluid of high Schmidt number (which it almost invariably is), there are almost no time lags of transfer rate associated with a change in convective rate. Thus the resolving power of this technique should be potentially higher than that of heat transfer experiments.
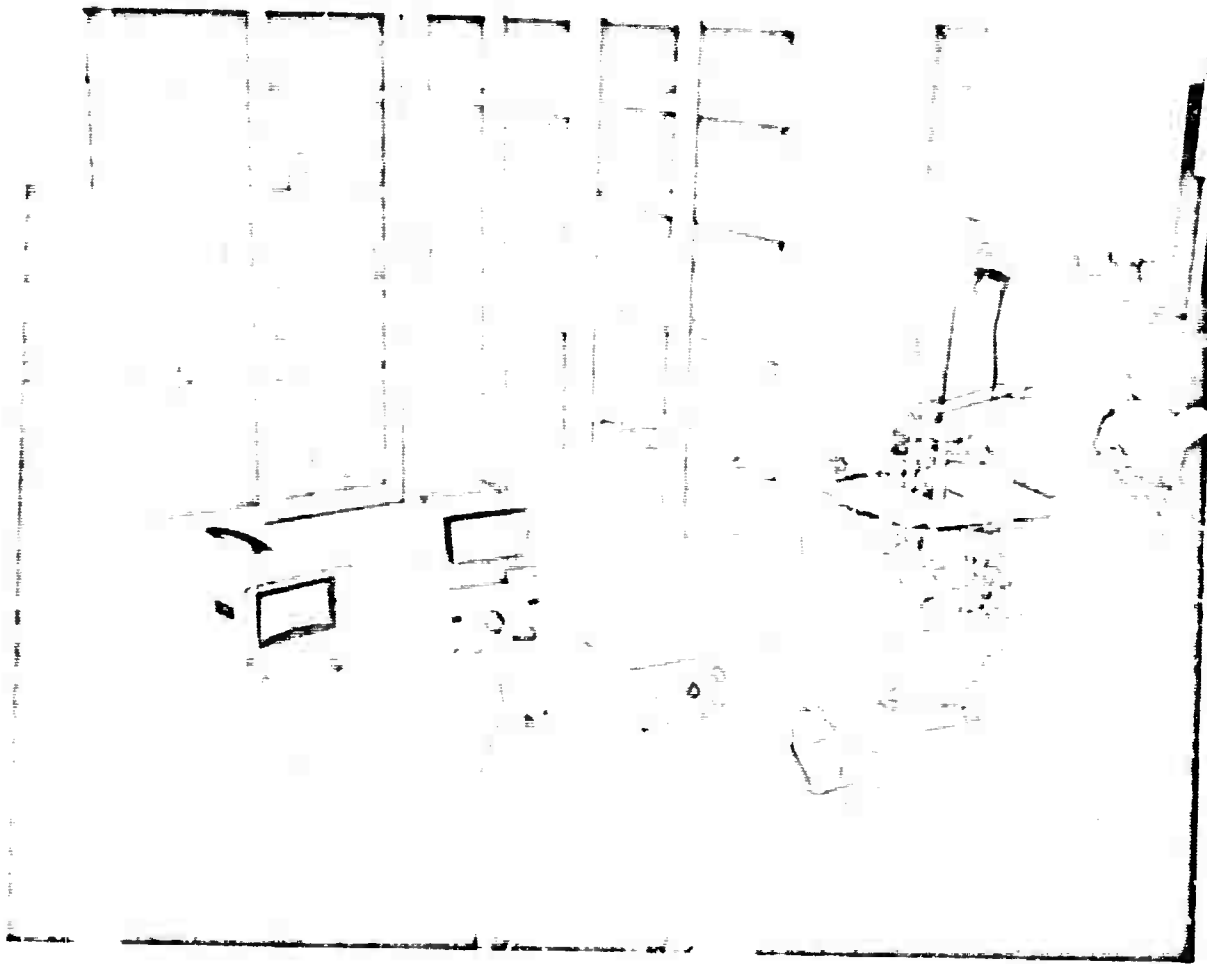
(*) i.e. Froude number

FIGURE 3 EXPERIMENTAL EQUIPMENT

3.3-2 <u>Electrodes</u>

Initially a solid, metal cylindrical electrode (1/8" diameter) was used. The metal cylinder was coated with an insulating lacquer and a slit about 1 cm long by 0.15 cm wide was cut in the lacquer. This then formed an active electrode area the size of which was known with reasonable accuracy. However, once the electrode carrier / assembled only a single angular orientation could be tested at a time. The test surfaces were usually made of one of the noble metals, so that this mode of construction was also rather expensive. Finally, none of the insulating lacquers used would last very long under actual test conditions.

Later "Bakelite" and "Ebonite" carriers of various diameters were developed. These had axial groves milled, into which wires of the test electrode material were glued with epoxy resin. An active electrode area was then obtained by grinding a length of about 3/4 inches of carrier length in such a manner that a fresh metal surface lay bare on the cylinder envelope. These test pieces were inexpensive and sturdy, and the number of angular orientations which could be tested without dismantling the rotating arm assembly depended only on the number of axial groves which could be conveniently milled in the carrier. There was however one disadvantage in that the active test area was not known accurately and thus calibration tests had to be run.

Electrode materials used were annealed gold, platinum and nickel wires. The wires were of 0.010" to 0.025" diameter. The counterelectrode was an annealed platinum foil on all test runs.

One of the objects of the study here reported was the study of flow conditions in regions of separated flow behind bluff bodies immersed in a flow. In particular, it was hoped that the degree of stabilization achieveable by splitter plates piaced downstream of the electrode carrier could be demonstrated. Accordingly several carriers with attached splitters were produced, at first with stainless steel vanes coated with an epoxy resin, later with platinum vanes. Electrode carrier construction and a carrier with vane are shown in the plates, figures (4) and (5).
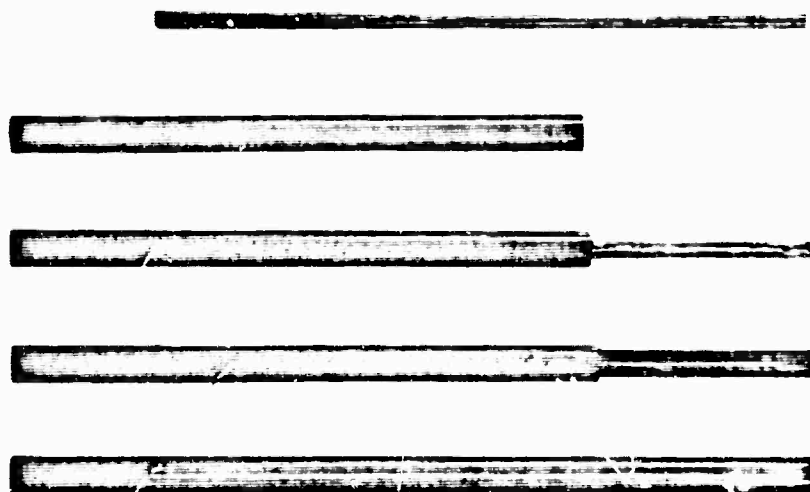
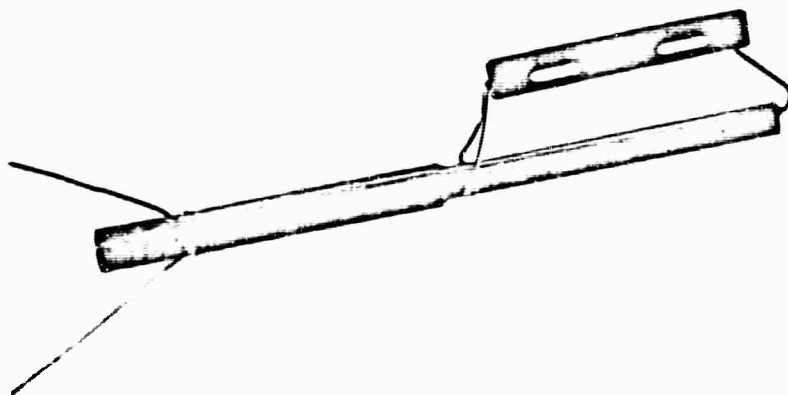FIGURE 4 CONSTRUCTION OF TEST ELECTRODES

FIGURE 5 TEST ELECTRODE WITH VANE

3.3-3 Preparation of the test electrode surface

For the first test series, using the oxygen reduction reaction on a gold surface, no preparation apart from cleaning of the gold surface with an organic solvent was undertaken (Dr. P. Stonehart). For the last of the hexacyanoferrate series the activation procedure used by the Zürich team (Ibl, [23]), was employed: after each test series the surface of the electrode was first ground to a smooth finish, whereupon electrode and carrier were cleaned briefly in trichloroethylene and rinsed in distilled water. The test electrode was then electrically cycled for about 5 minutes in a solution of about 10 ppw KCN, 30 ppw Na_2CO_3, 30 ppw KOH in 500 ppw of aqua. The test electrode was connected cathodically and the applied voltage was raised until gas evolution took place. The electrode thus prepared was rinsed and immersed in the test bath.

The counterelectrode and the free convection foils were similarily prepared.

3.4 Measuring equipment

3.4-1 The reference electrode

A standard mercury pool type reference electrode was used in order to measure the potential difference between the test electrode surface and the solution. For the first test series a calomel solution in KCl was used for contact with the mercury, later HgO (mercuric oxide) in NaOH. In order to reduce the diffusion of mercury salts into the test bath a special type of test electrode holder was developed, figure (6).

The voltage between reference electrode and test piece was measured at no current, by an instrument with a 100 $M\Omega$ input impedance.

3.4-2 The current was measured by inserting a low impedance galvanometer in the return from the test electrode. The period of rotation was measured by electrical timers which were first calibrated.

The accuracy of the instrumentation used finally exceeded by far the accuracy and reproducibility of the system as a whole, so that a detailed analysis of measurement error did not seem to be warranted.

3.5 Data reduction

3.5-1 Theory of electrochemical process

SATURATED SOLUTION
HgO + NaOH

HgO

Hg

Pt WIRE

SIN _RED GLASS
FILTERS
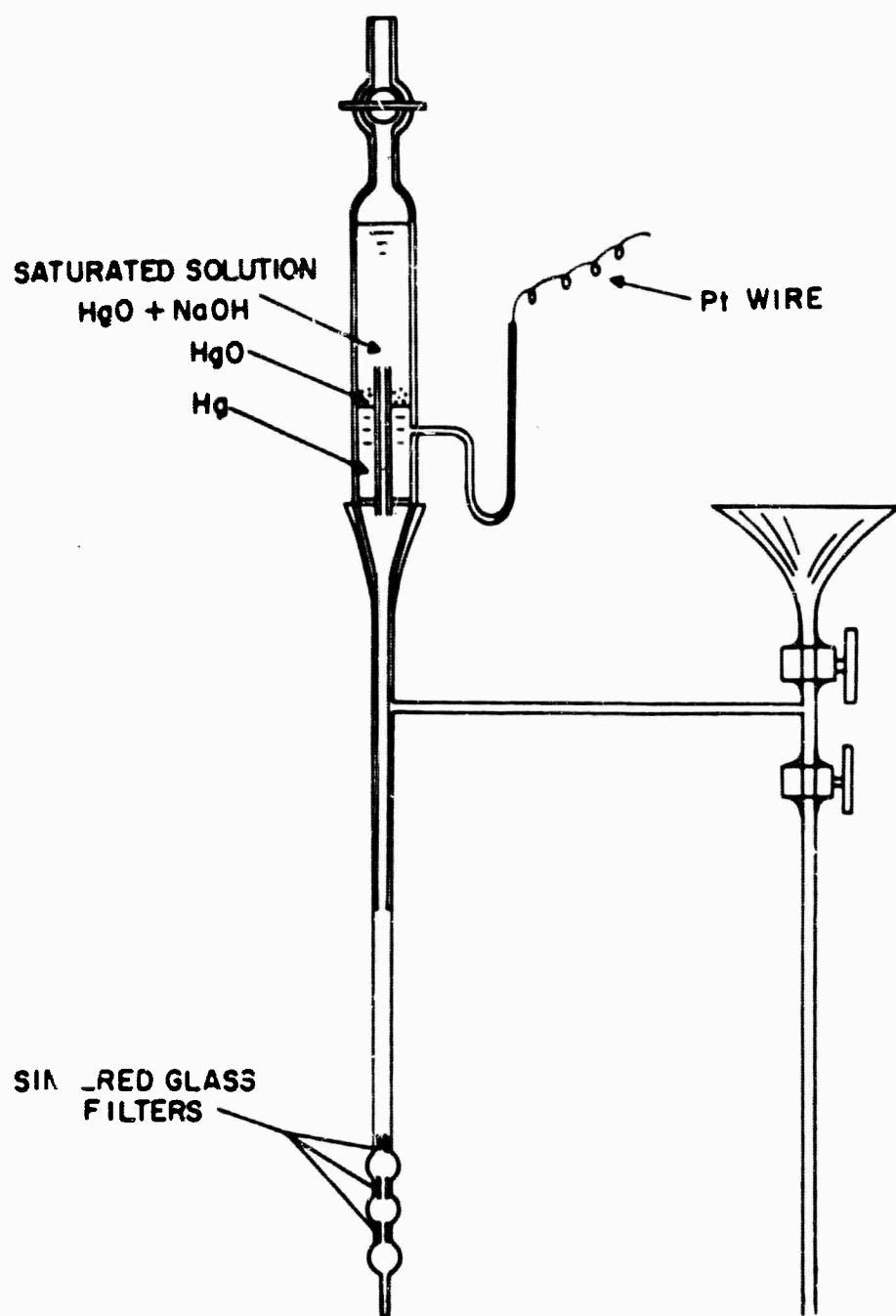
FIGURE 6   REFERENCE ELECTRODE AND ELECTRODE HOLDER.

Assuming a single reaction at the test electrode surface, the transfer-rate is given by the following expression:

$$TR = \frac{i''}{F \times N_v} \qquad \ldots (3.1)$$

where i'' is the interface current density; F is the Faraday constant and N_v is the reaction valence. The mass-transfer coefficient is obtained as follows:

$$H = \frac{TR}{c_\infty - c_o} \qquad \ldots (3.2)$$

where c_∞ is the concentration of the active species in the bulk fluid and c_o is the interface concentration. This latter value is commonly assumed to be zero for reactions proceeding at a fast rate. An expression for the mean Sherwood number is obtained by inserting (3.1) into (3.2):

$$\bar{Sh} = \frac{I \cdot l}{A \cdot (c_\infty - c_o) N_v F \mathcal{D}} \qquad \ldots (3.3)$$

where I is the current measured; l is a reference length; A is interfacial area and $\mathcal{D}$ is the diffusion constant.

3.5-2 Calibration tests

For most of the test conditions neither the interfacial area nor the diffusion constant were known with great accuracy à priori. Independent calibration tests were therefore run as follows. The diffusion constant was determined by measuring the natural convection mass transfer rates on platinum foils of accurately known dimensions, suspended vertically in the fluid. For this case the mean dimensionless transfer coefficient at large Sc number is given by,

$$Sh = 0.653 (Gr \cdot Sc)^{1/4} \qquad \ldots (3.4)$$

where the reference length l is plate height.

Inserting (3.3) for $\bar{Sh}$ and solving for $\mathcal{D}$,

$$\mathcal{D} = 0.7009 \cdot \left(\frac{I}{b \, l \, F \, N_v \, (c_\infty - c_o)}\right)^{4/3} \left(\frac{\nu \, l}{g \, \Delta \rho / \rho}\right)^{1/3} \qquad \ldots (3.5)$$

where b is plate width. Or, in dimensionless forms,

$$\frac{\mathcal{D}}{\gamma} = 0.7009 \ Gr^{-1/3} \left(\frac{I}{b \ N_v \ F \ (c_\infty - c_0) \ \gamma} \right)^{4/3} \qquad \ldots (3.6)$$

Usually, at least two tests were run, using plates with different dimensions. Values of Gr obtaining in practice were in the range 4×10^4 to 3×10^5 In order for the asymptotic, boundary layer type theory outlined above to be applicable, we must have,

$$Sc > 10^3 \ ; \qquad 5 \times 10^4 < (Gr \cdot Sc) < 10^9$$

The upper limit on $Gr \cdot Sc$ is introduced by the onset of transition to a turbulent boundary layer. Also, in order to reduce three-dimensional flow effects, the ratio: foil height to foil width, $\mathcal{L}/b$, should be smaller than $1/4$.

In order to be able to evaluate the Grasshof number at test conditions, a knowledge of the change in density taking place at the test electrode surface is necessary. The relevant data for the system here used, but at different concentrations, have fortunately already been previously reported [24]. The accuracy of which the experiment described here was capable did not warrant an independent detailed check of these data. which can be done by using the method of Fouad and Ibl [25], and interpolation data between the reported test points [24] were used.

The kinematic viscosity of solutions of the composition and concentrations used in the present series of experiments has previously been reported (c.f. [20], p. 530), but these were in part repeated independently.*

Once the Schmidt number was known, the test electrode area was obtained by assuming equation (2.6) to be applicable at the front stagnation point when the test electrode is measured in forced convection. Insertion of -

$$\left. \begin{array}{l} \beta \ (x) = 3.4865 \ \frac{x}{R} = 3.4865x \\ x^* = 0 \end{array} \right\} \qquad \ldots (3.7)$$

into (2.6), (2.6a) and comparison with eq. (3.3) yields,

$$\bar{\beta} \ (x) = \frac{4}{9} \ \beta \ (x)$$

$$A = 1.069 \ \frac{I. \ R}{C \ N_v \ F \mathcal{D}} \cdot Re^{-1/2} \ Sc^{-1/3} \qquad \ldots (3.8)$$

---

* Values found: γ=1.325 centistokes at 23 °C; 1.267 at 25; 1.212 at 27; ρ = 1.090 at 23.9 °C Grassmann et al. 24 reported a value of γ=1.26 centistokes. See also Appendix III.

3.5-3 The direct measurement of wall shear stress

Once both the diffusion coefficient and the interfacial area have been determined the local wall shear rate at locations away from the front stagnation point may be obtained directly by eliminating $\bar{S}h$ from equations (2.6) and (3.3) for the constant wall concentration case:

$$\beta(\bar{\jmath}) = \left(\frac{2\Gamma(\frac{4}{3})R}{A\ F\ N_v \bar{\wp} \Delta c} \right)^3 \cdot \frac{\Delta\gamma}{3\ Sc}\ \frac{I^3}{Re^{-\frac{3}{2}}} \qquad \ldots (3.9)$$

3.6 Results

The graph figure (7) shows an example of a polarograph obtained during one of the first test series with the oxygen on gold reaction. It will readily be realized that there is no real limiting current "plateau" and that the effect of cycling hysteresis is very notable. This latter phenomenon may have been due both to continuous change in oxygen saturation, or rather supersaturation, on the one hand and surface activation, later counteracted by surface poisoning, on the other.

The graph, figure (8) shows an example of polarograph obtainable with hexacyanoferrates redox reactions and with a reasonably clean technique. When quite fresh, electrode active areas may yield limiting current "plateaux" which extend virtually from +0.25 to -1.0 volts without a noticeable change in the value of the current passed.

The graph, figure (9)[*] gives transfer rates for a system of which graph (8) represented the polarograph. It is seen that the front stagnation point transfer-rate values (marked FSP on the graph) follow the theoretically expected line within a reasonable amount of scatter. Surprisingly, though, the values for the rear stagnation point (marked RSP) also fall on a line with slope $1/2$ in the log-log plot. Values for an angle of $\pi/2$ fall _above_ those for 0° and for π, as expected from the theory (equation 2.6 above).

In the graph figure (10) results are given for the case of cylindrical electrode

---

[*]Figure (9) is not directly comparable with the following figures due to the different concentrations of chemicals used.

FRONT STAGNATION POINT TRANSFER RATES

GOLD ELECTRODE IN NaClO₄ SOLUTION

Ph ≈ 7.0, b = 22.7°C, Mk II RIG

NOTE "DOUBLE PLATEAU" EFFECT

VOLTS →

GRAPH FIGURE 7

POLAROGRAPH, TEST SERIES XIII

VOLTS

GRAPH FIGURE 8

TEST RUN ON Mk X I RIG

UNSTABILIZED FLOW: SEPARATION NEAR π/2

POINTS TAKEN IN WRONG ORDER, AS CHECK

0°	×	
180°	✳	
FAULTY RUN	⊕	
90°	·	

φ = π/2

F.S.P. SLOPE 1/2

R.S.P.

TRANSFER RATE, μ COULOMBS/(sec × cm²) × 10²
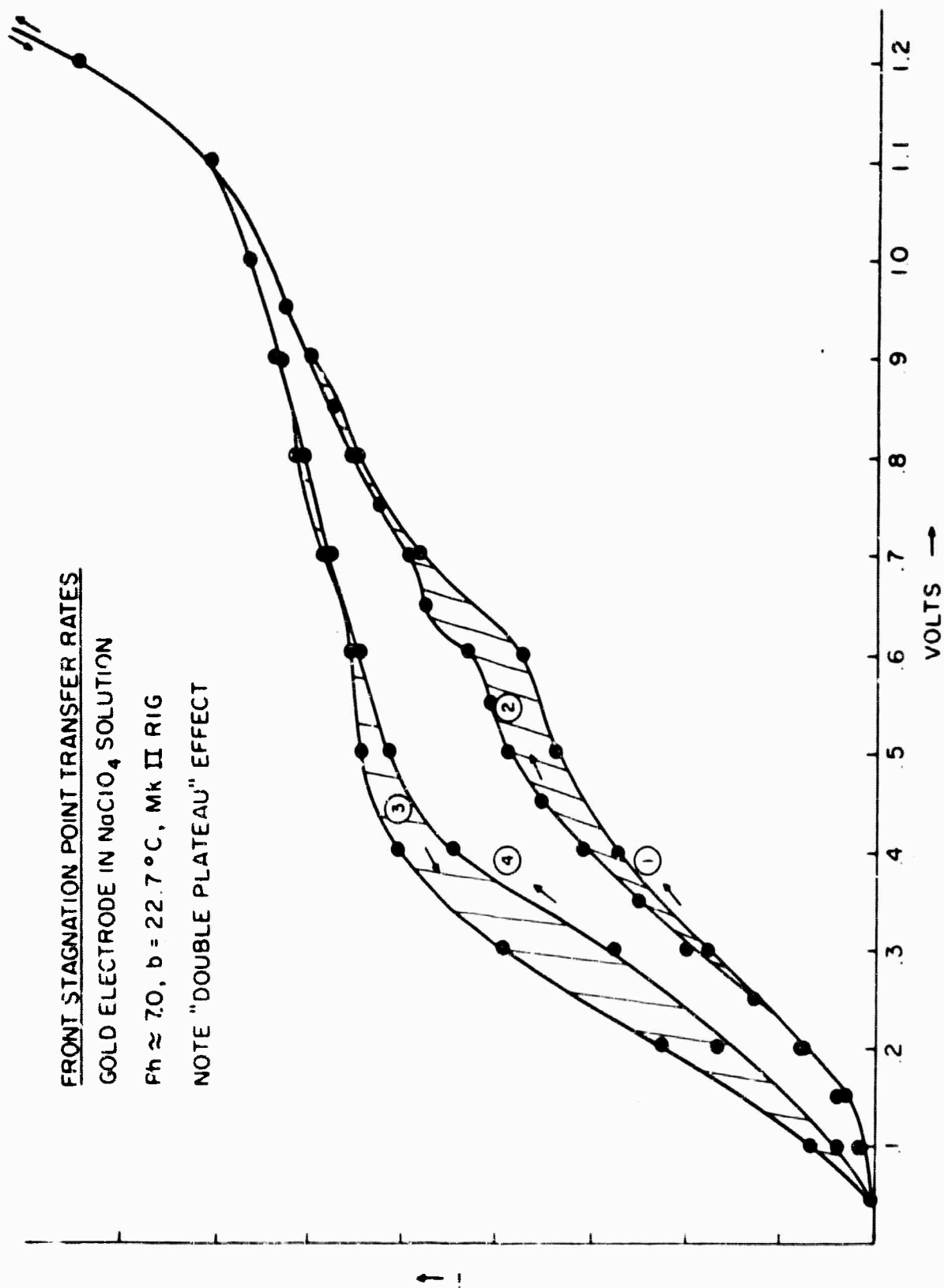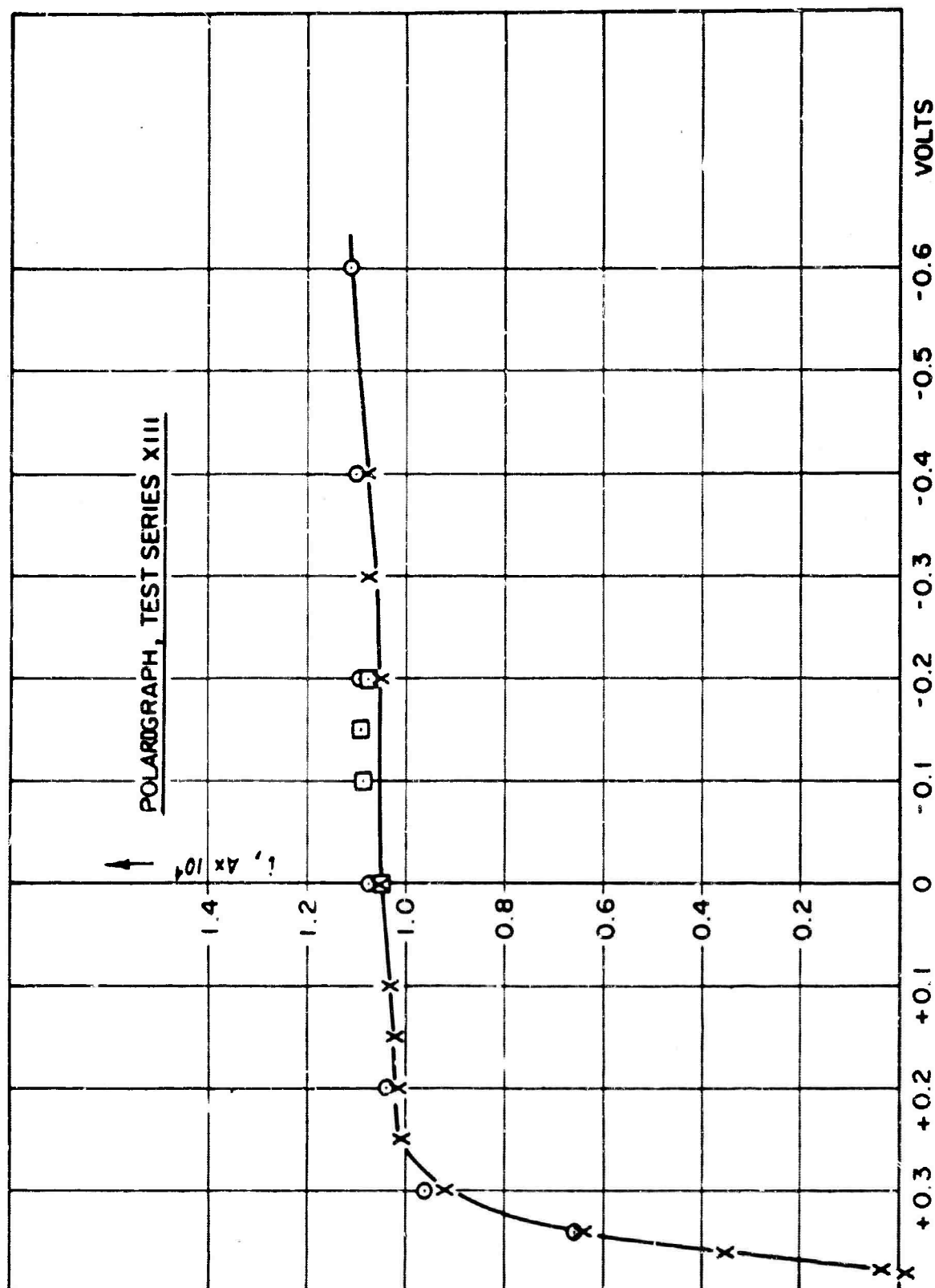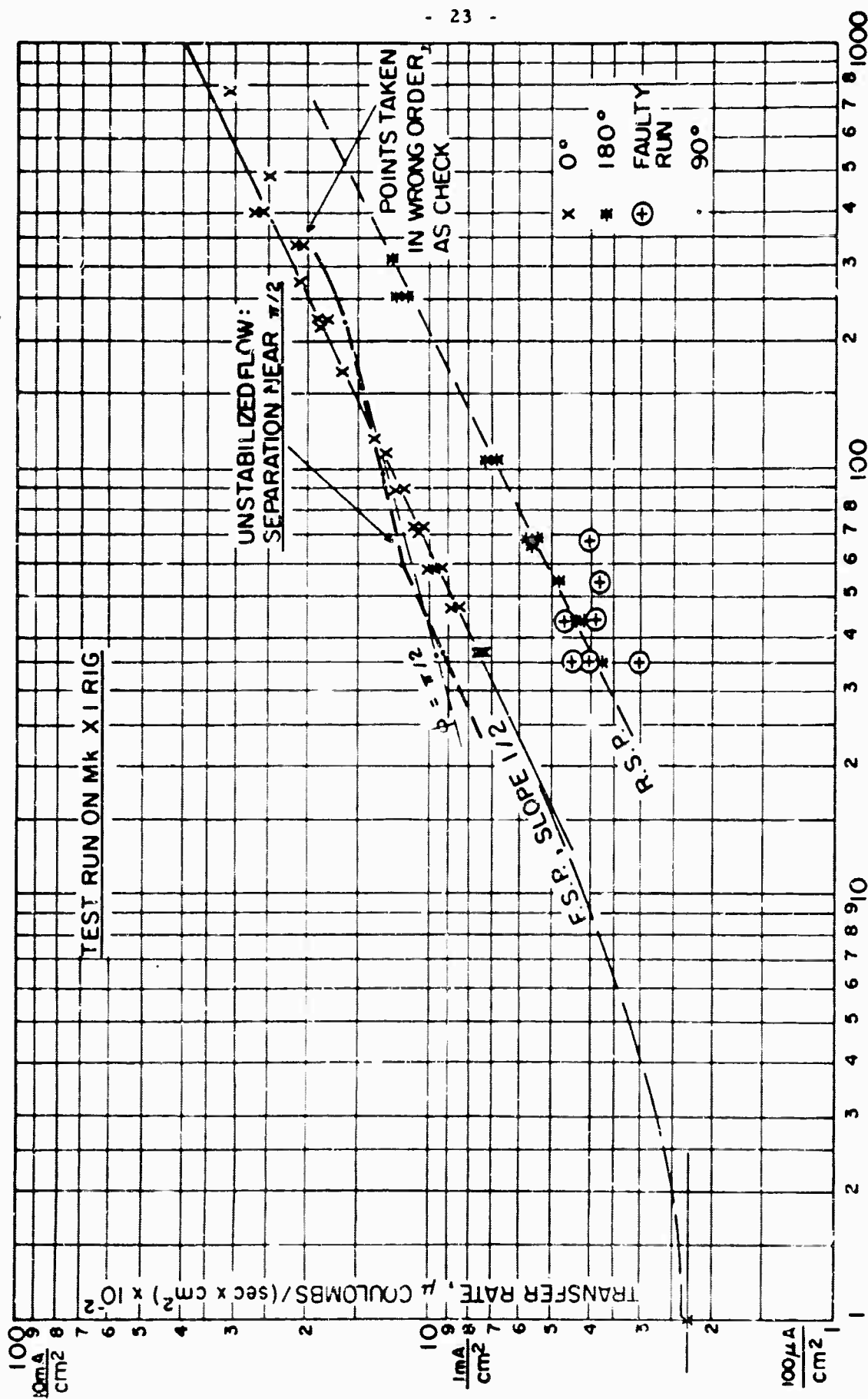
$Re_d \longrightarrow$

GRAPH FIGURE 9

carriers with and without a stabilizing vane attached to their downstream side. The plate figure (5) showed an electrode carrier with attached stabilizing vane. It is seen from graph (10) that the level of transfer densities is reduced when the electrode carrier with a vane is tested, as compared to the same carrier when the vane was cut off. The character of the curves is, however, not altered.

Figure (11) illustrates the results when the electrode carrier with vane attached is rotated in the opposite direction, so that the vane faces upstream. Predictably, transfer rates are reduced, at what is now the F.S.P., in the low Reynolds number range, as the F.S.P. electrode is now bathed in the viscous wake from the upstream splitter vane and local wall shear-rate values are reduced. At high Re, however, transport rates are increased: this may be attributed to the fact that the upstream splitter vane sustains a non-zero angle of incidence to the flow, and thus a sizeable velocity from the pressure side of the plate to the suction side may sweep past the electrode surface.

The graph figure (12) shows complete results of test series XIV giving values of transfer coefficients at various Reynolds numbers, with the angle substended to the flow as a parameter. The small amount of scatter obtained is notable.

3.6-1 Comparison of the experimental results with the theory of para. 2.1-1

In the graph, figure (13) the results given in the previous figures are re-drawn so as to give the ratio of Sherwood number to (Sherwood number with the mass transfer strip at the front stagnation line), plotted versus the circumferential angle substended by the median of the strip, and with the Reynolds number as a parameter. Also drawn in the graph is the result obtained from equation (2.5) based on the following:

An experimentally determined velocity distribution around a cylinder in stabilized laminar channel flow has been obtained by Grove [29], and his data may be correlated by the following, Acrivos [30],

$$u^2 = 3.758\varphi^2 - 2.84\varphi^3 + 0.574\varphi^4 \qquad \ldots (3.10)$$

Here the velocity u has been rendered dimensionless by using as reference velocity the value obtained within the channel at the location of the cylinder before the latter's insertion. In view of the fact that the blockage ratio of the

TEST RUNS ON Mk XIII RIG

- 25 -

GRAPH FIGURE 10

TRANSFER-RATE, m COULOMBS/sec x cm²)

Re_d →

TEST RUNS ON Mk XIII RIG

TRANSFER RATE, m COULOMBS/(sec x cm²)

Re$_d$ ⟶
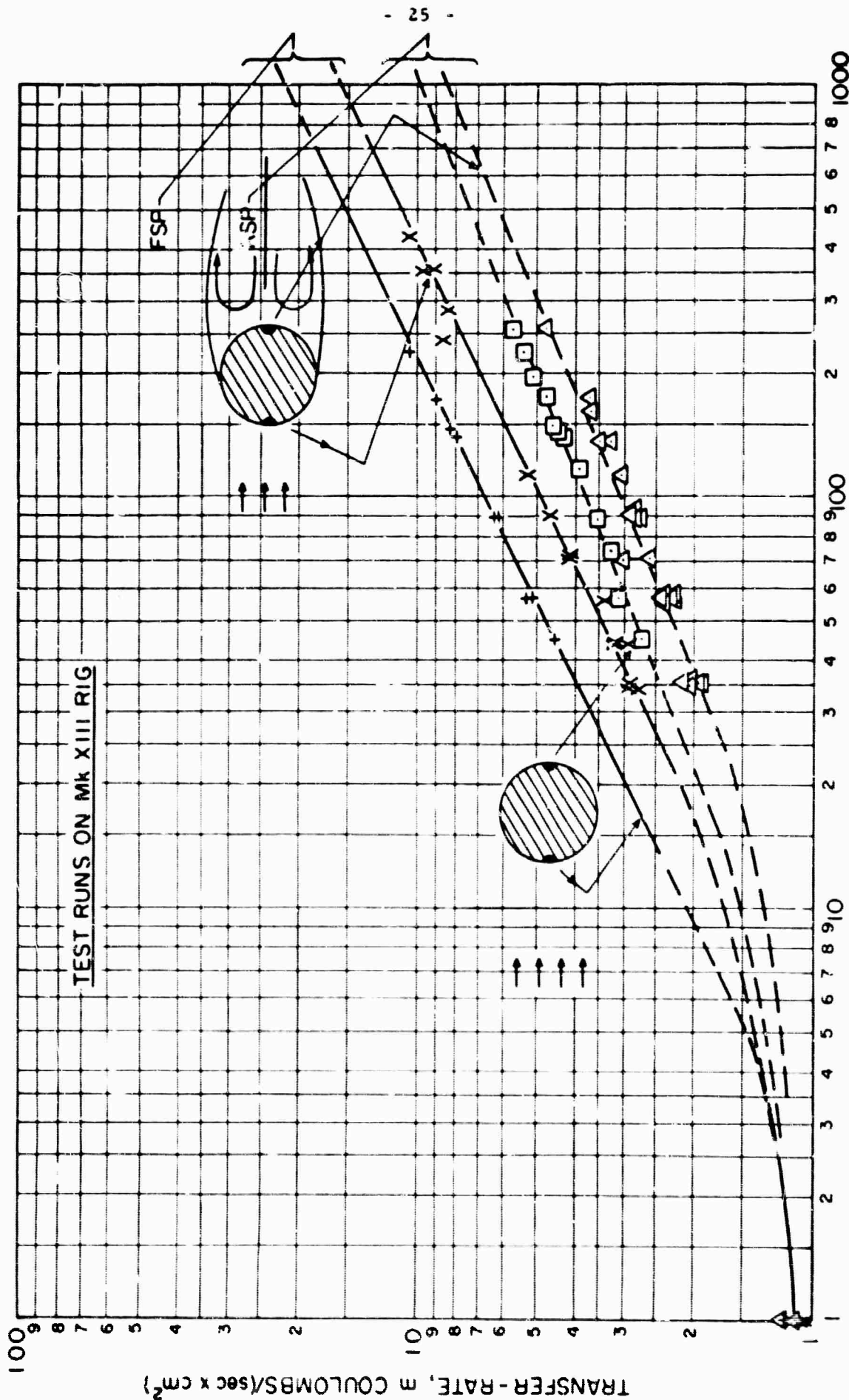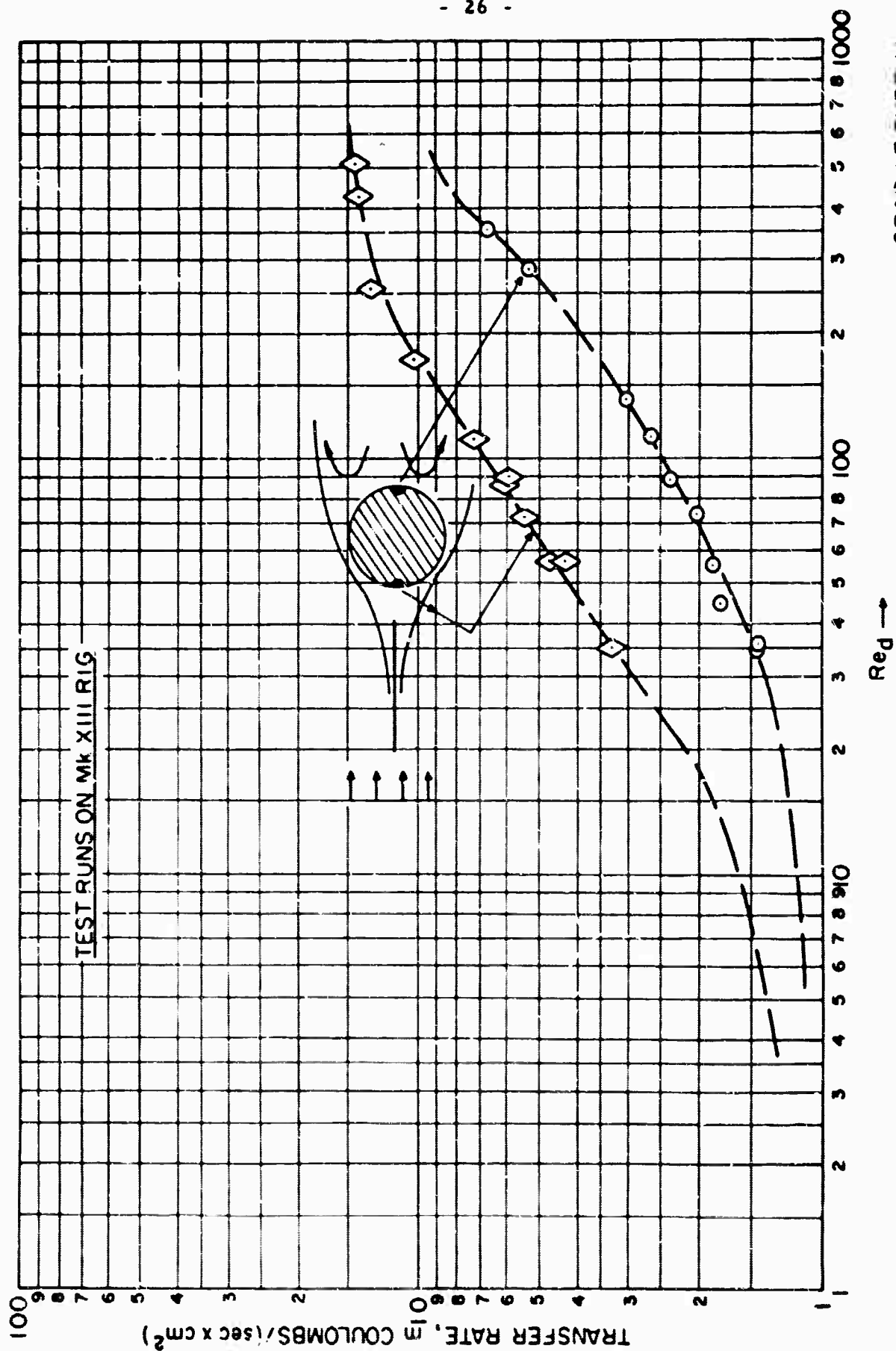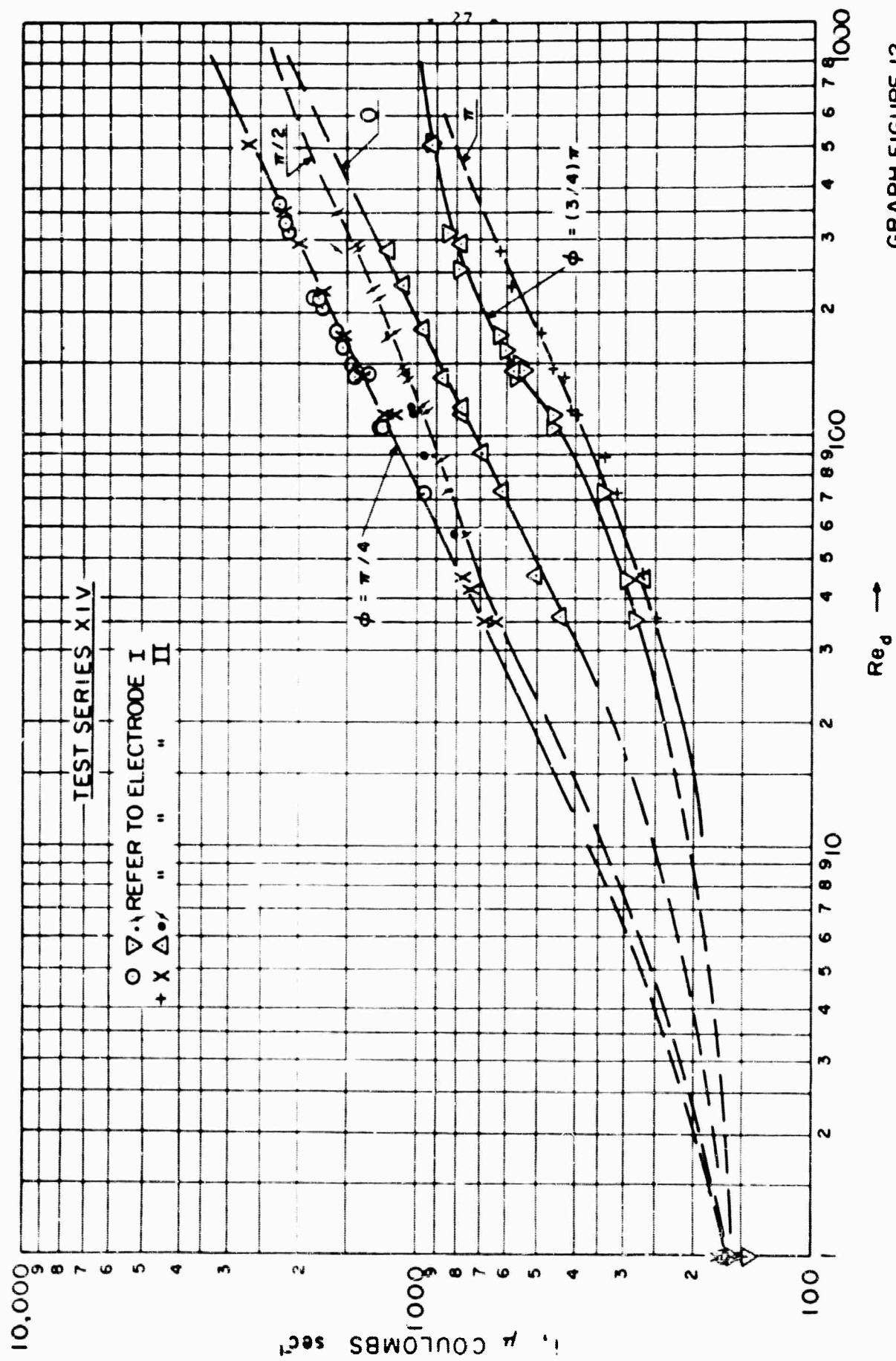
GRAPH FIGURE 11

GRAPH FIGURE 12

DISTRIBUTION OF MASS TRANSFER COEFFICIENTS AROUND CYLINDER FOR SOURCE WIDTH OF 11.6°
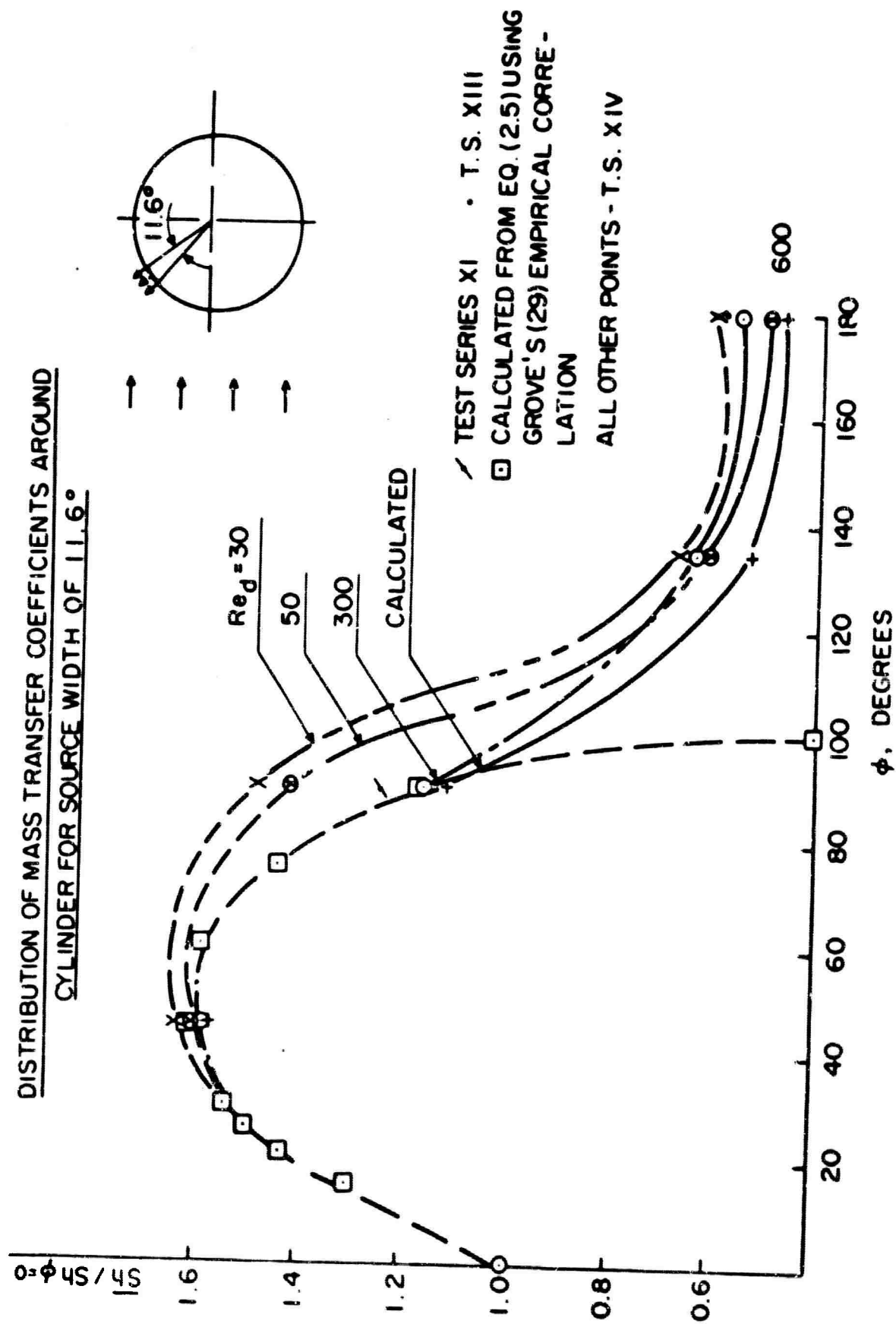
GRAPH FIGURE 13

channel was appreciable,(3.10) cannot, of course, be taken to represent a good correlation for the widely differing case here considered. Another esthetical flaw is that (3.10) is not symmetrical with respect to φ.[*] It was used nevertheless, as there are few reliable experimental data available.

From (3.10) the local shear stress at the wall may be calculated using one of the approximate methods. We used here that of Acrivos [13] and obtained,

$$\beta(\varphi) = \varphi \left[4.97 - 4.84\varphi + 1.157\varphi^3 \right]^{3/4} \qquad \ldots (3.11)$$

The values of β thus obtained may be introduced into equation (2.5) together with the requisite source-strip width (11.6 degrees in the present case) to give an estimated curve of the circumferential distribution of mass transfer coefficients. It is seen from the graph, figure (13), that there is fair agreement over that part of the cylinder circumference where such an empirical relation could be expected to yield reasonable results, id est not too close to the boundary-layer separation point. The results plotted in graph (13) thus give us some confidence in using the experimentally determined mass transfer data in order to estimate wall shear rates in the range 92° to 180° where no other direct measurements have been available heretofore.

3.6-2 Critique of method and suggested improvements

The main difficulties experienced were electrochemical in nature: (a) the diffusion coefficient found from our free convection experiments is rather low compared to that reported by other investigators. The value found here was 3.1×10^{-6} cm^2 sec^{-1} in test series XIII; 3.58×10^{-6} at 21°C and $4.13 \times 10^{-6}$ at 25.3°C, in test series XIV. The value reported by Grassmann and coworkers is 5.8×10^{-6} at 25°C;[+] (b) after a very short time of operation the response time of the system to altered conditions of speed or driving force (E.M.F.) became very large indeed. Once the surface had thus deteriorated, values of current measured under any given conditions were invariably higher than the true steady-state values obtained with a fresh surface; (c) it would appear likely that in order to obtain consistently reproducible experimental data a continuous activation of the test electrode surface by superposition of an A.C. component on the D.C. passed through the system is necessary.

---

[*] The use of the absolute value for the second term would render the function non analytical. Similar remarks apply to equation (3.11).

[+] See also Appendix III.

TEST SERIES XV POLAROGRAPH WITH NICKEL ELECTRODE

GRAPH FIGURE 14.
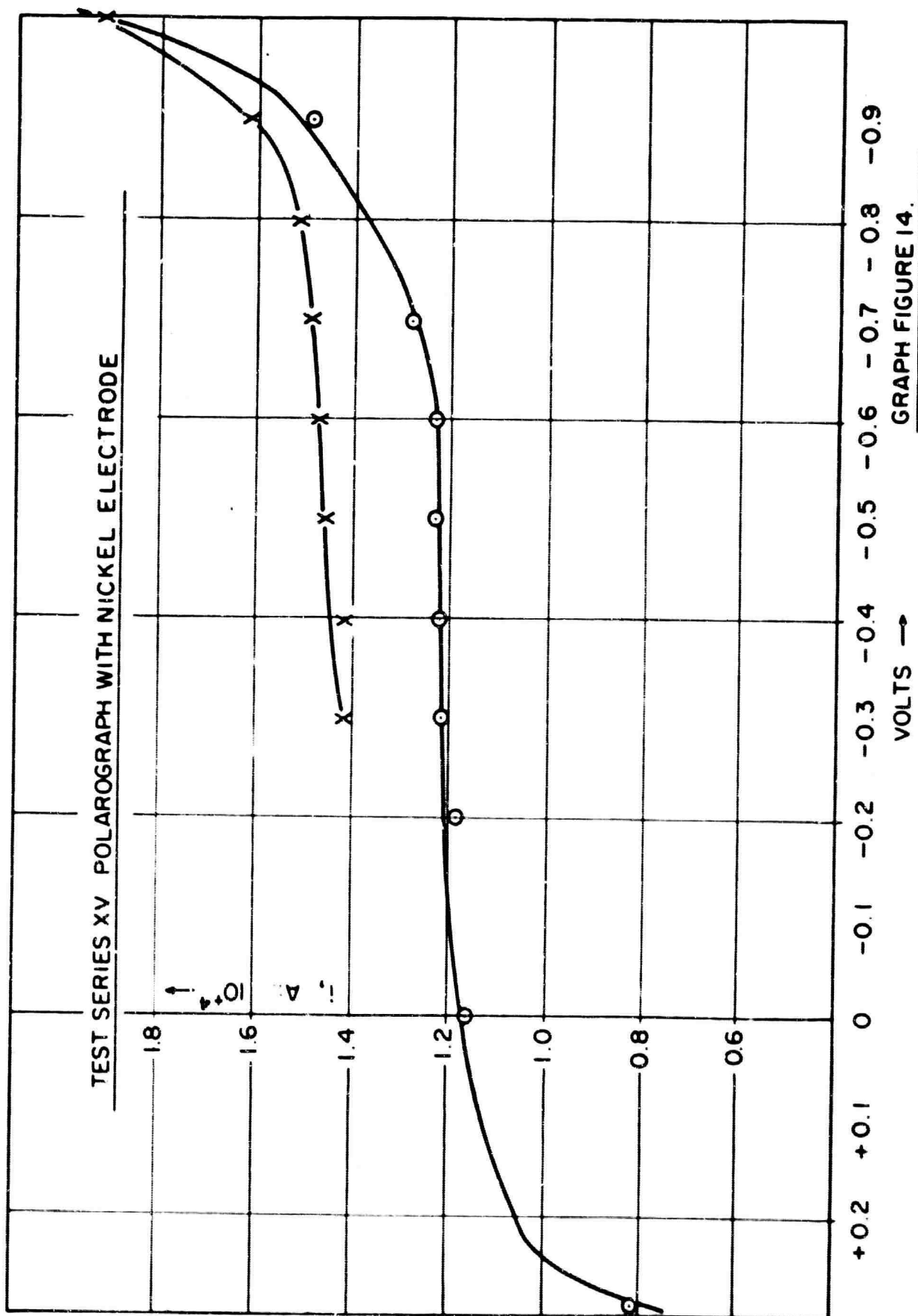
3.7 The frequency of Kármán Vortices shed behind blunt objects in an essentially two-dimensional flow

As pointed out in section 3.3-1 the electrochemical system described measures transfer-rate oscillations, with amplitude and frequency distortions which can be made arbitrarily small by choosing suitable measurement instrumentation. Thus it is singularily well suited to the measurement of the vortex shedding frequency behind blunt objects placed in a stream, when the monitoring electrode is placed near the rear stagnation point: the oscillatory frequency in the current measured corresponds to a synchronous oscillation in the local shear-rate at the wall.

It is shown in classical work that the oscillatory frequency can be correlated with the linear dimensions of the obstacle, the fluid velocity and fluid kinematic viscosity in a unique way:

$$S = F (Re) \qquad \qquad \ldots (3.12)$$

where S is the Srouhal number, $S = f.1/U_\infty$, with f equal to the frequency; 'l' a characteristic length (usually the greatest extent of the body in a direction perpendicular to that of the flow velocity at great distance from the body, U_∞); and Re is the Reynolds number. The functional relationship (3.9) cannot be determined from analysis and must be found from tests. However F is very little dependent on the detailed cross-sectional shape of the blunt body tested.

In the graph, figure (15) measured values of frequency (obtained by timing the oscillation of the current observed on the galvanometer in the test electrode circuit) are compared to data reported by Roshko, [26], [27], and by Shair, [28]. Shair's data are apparently not very reliable [30] as in his tests the velocities were incorrectly measured; however, in conjunction with Roshko's very careful measurements and the data reported here, they seem to indicate that at any given Reynolds number at which instability does indeed take place, the Srouhal number is the higher the larger the channel blockage ratio. This result cannot be taken too seriously without much additional careful testing.

Another interesting point apparent from graph (15) is that while the stabilizing vane did not suppress instability of the wake within the range of Reynolds numbers where it was expected to do so, it nevertheless reduced gross turbulence somewhat and thus gave rise to lower Strouhal numbers. The same effect was found by Roshko, [27].

STROUHAL NUMBERS TEST SERIES XI

0.30

STROUHAL NO

0.28

0.26

0.24

0.22

0.20

0.18

0.16

0.14

0.12

0

5.0

100

150

200

250

$Re_d \longrightarrow$

SHAIR*

ROTEM
X

ROSHKO

$d/h = 0.175$

$d/h = 0.200$

$(d/h)_{eq} \simeq 0.04$

TEST SERIES XI

X–X

SCATTER

SCATTER

ROSHKO, NACA TN 3169

X   T.S. II
△   T.S. 13
⊠   √ WITH VANE
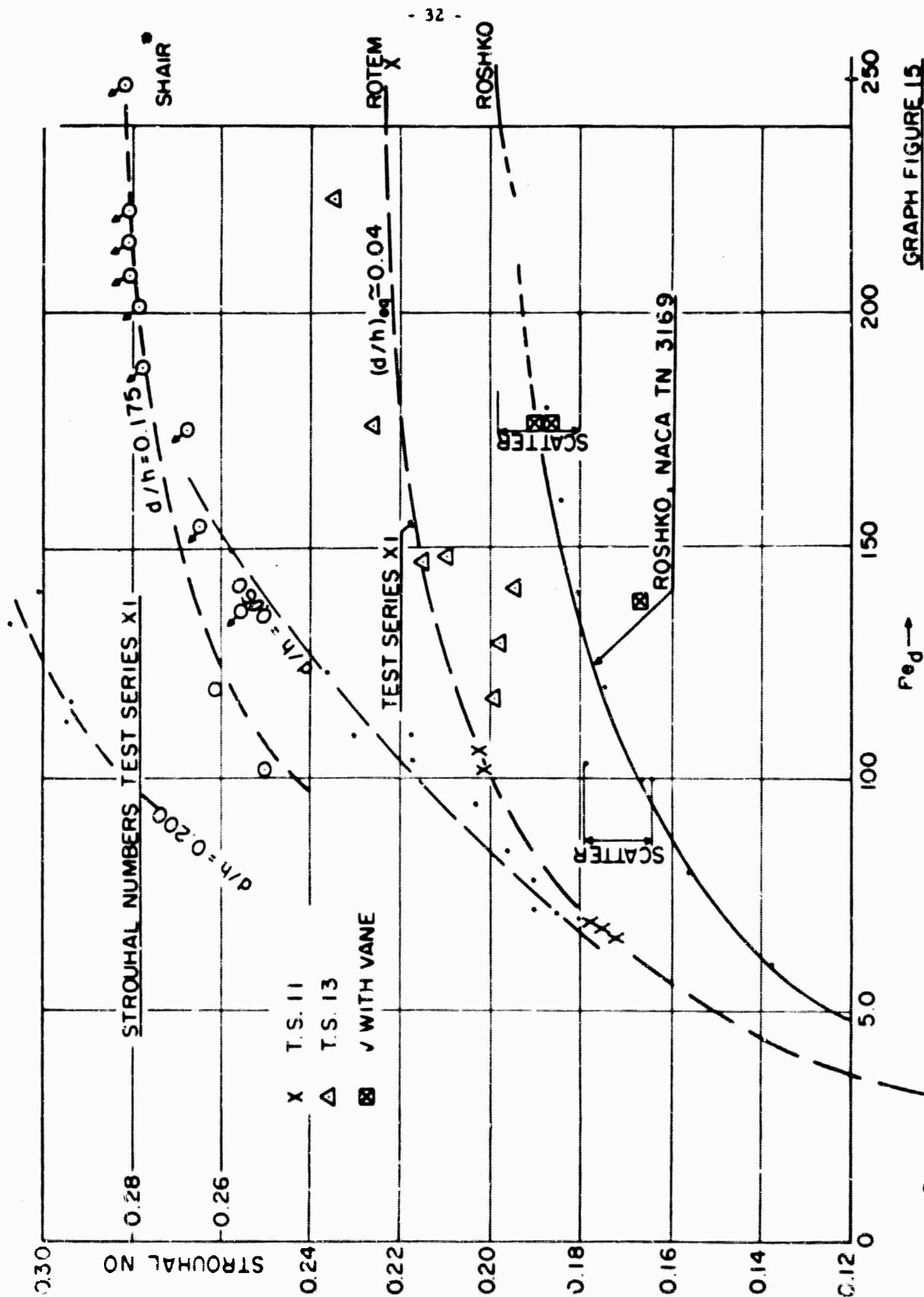
GRAPH FIGURE 15

* Re given by Shair increased 25% to allow for incorrect data; results on this graph show sliding scale should be used.

4. Experimental: Heat Transfer Studies

4.1 Introduction

It was pointed out in sections 3.1 through 3.2 above, that the initial expectations were that the electrochemical mass transfer studies would yield rapid and accurate results with little expenditure and complication. From the exposé in section 3.6 it will however have become clear that the accuracy and the reproductibility of these experiments were rather worse than one was led by electrochemists to believe. Also, no conclusive evidence of the degree of stabilization achievable with the splitter plate, and the influence of this stabilization on RSP mass transfer rates for flows with very low blockage ratios was forthcoming. So it was decided to run some equivalent heat transfer studies.

A closed circulation laminar-flow oil tunnel was available in the Department and has already been described previously [14], [15], [17], [28], [29], [31], [32]. It is apparent from those previous studies that this oil tunnel may not be an ideal research tool for the study here proposed due to some uncertainty in the interpretation of previous experimental data (compare [28] through [32]). Enough is nevertheless known about the variation of the rates of shear on the wall of a test cylinder placed in that tunnel, at least up to the point of boundary layer separation. Thus data to be measured in that region may be used for calibration purposes.

4.2 Construction of heat transfer cylinder

The diagram figure (16) and plate (17) show the construction of the heat transfer cylinder with a strip heat source. Outer diameter was 3/4 inches nominal. It will be seen that this cylinder is of simple, rugged and cheap construction.[*] The heating surface consisted of a carefully rolled copper strip, 1/16 inch wide and 0.009 inches thick. It was embedded in a grove cut parallel to the cylinder generating line. The copper heating strip was

[*] The help of the Mechanical Workshop of the Chemistry Department in the construction of the heat transfer cylinder is gratefully acknowledged.
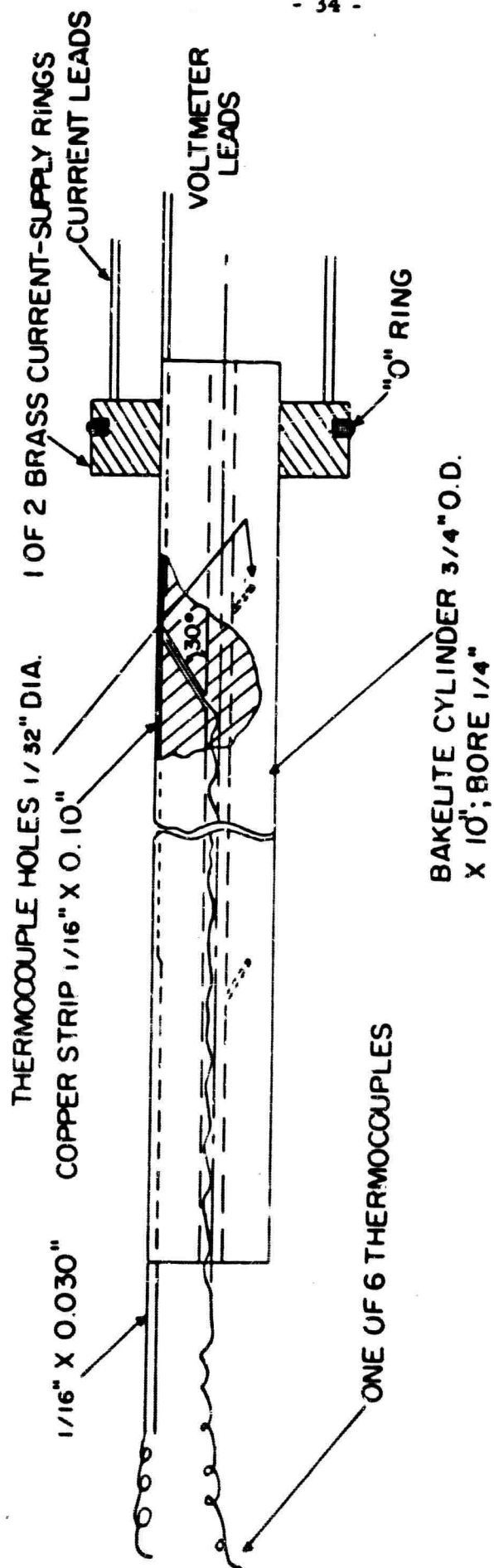
FIGURE 16: STRIP HEATED H. T. CYLINDER
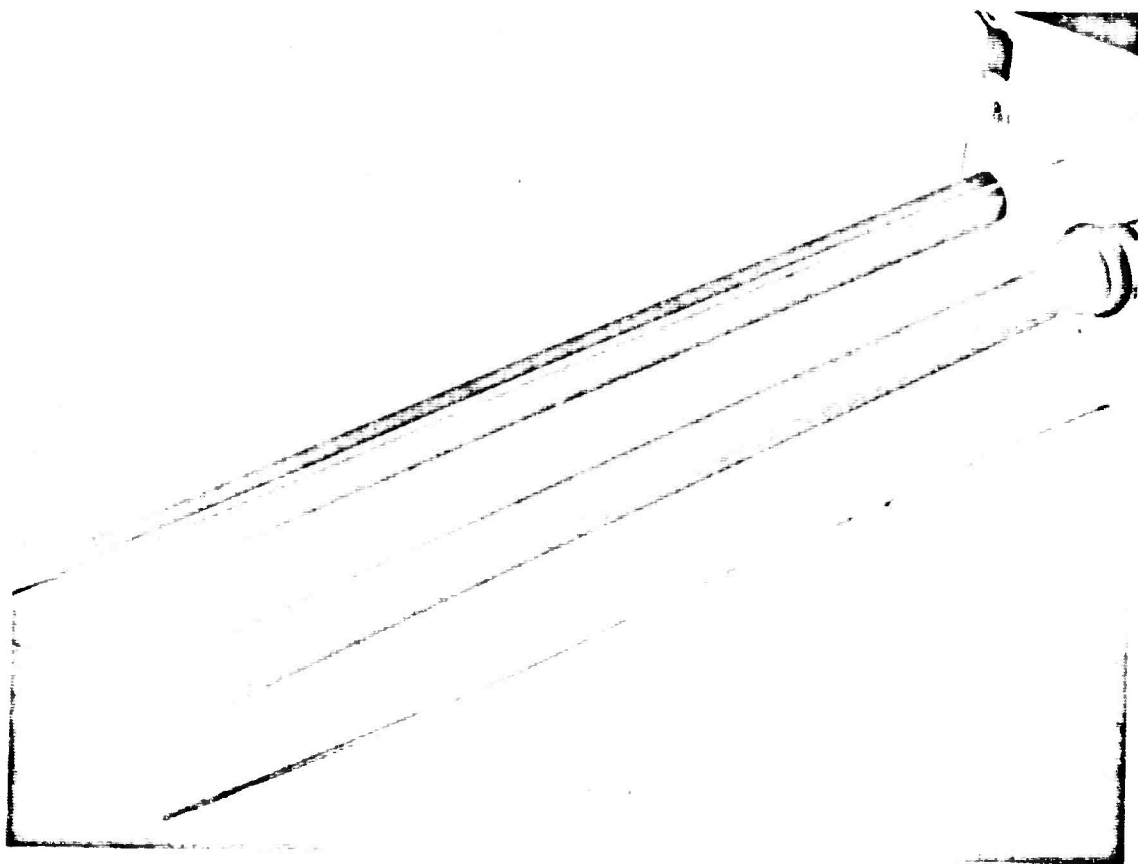
FIGURE 17 TEST HEAT TRANSFER CYLINDER

FIGURE 18 ASSEMBLED TEST CYLINDER

"short-circuited" over the terminal 1 inch near the channel confining walls, so that appreciable heating took place only over the central 6 inches of the channel. This was done in order to avoid end effects through the heating of the rather thick wall boundary layers. The short-circuiting was carried out by having the heating strip at 5 times its "central" thickness, and deepening the grove holding the strip correspondingly.

Three thermocouples were welded in the standard manner using copper constantan 32 BWG, fiberglass and enamel insulated wires. The cleaned junction was then silver soldered to the underside of the strip at locations dividing the heated length into quarters. The thermocouple wires were led to the central bore of the cylinder and thence to the measurement apparatus. Finally the heating strip was glued into place using an epoxy resin ("Araldite").

Three other thermocouples were prepared in the same manner and glued into countersunk holes at various circumferential locations on the cylinder envelope. These latter thermocouples served for the determination of the free-stream temperature.

At each end of the cylinder a heavy brass ring was shrunk with a slight interference fit over the otherwise assembled cylinder, and the heating strip was silver soldered to the rings. Thus a good electrical contact was assured. The brass ring served both for supply of the rather heavy low voltage current and for carrying "0" rings assuring a close fit of the cylinder in the channel walls.

4. 3 Measurement Technique

Current was supplied from a high current AC source[*]. The voltage drop over the heating strip was measured by connecting a very high impedance AC voltmeter to the brass current supply rings described

above. On a later build separate leads were soldered to the heating strip, so that only the voltage drop over the central 6 inches of strip was measured, making for greater measurement precision.

The resistance of the heating strip was deter ined by separate calibration. A constant DC current delivered by a potentiostat was measured by a precision H. P. milliammeter and passed through the strip. The voltage drop was measured with the aid of an electronic microvoltmeter (COHU-KAYLAB model 203). Values found: 7.41 milliohms for the active 6 inches of heating strip, and 12.9 milliohms between the supply clips, at an ambient temperature of 22.1 $^{\circ}$C.

Temperatures were measured in the usual way, using a separate cold junction connexion for each thermocouple. A Leeds and Northrupp K3 potentiometer was used, which enabled readings to be taken to 1 microvolt.

The tunnel test variables were measured as described in 28 and 29, and will be described in detail in $\left[32\right]^{(*)}$.

4.4 Results

In contradistinction to the mass transfer experiments described in chapter (3) above, the heat transfer experiments proceeded without fuss or running-in difficulties. Indeed, the very first calibration run yielded useful, consistent and reproducible results, figures (19) and (20). The test apparatus proved quite sensitive, and such detailed features as the slight variation of transfer coefficients inside the stabilized wake bubble with change in attitude angle or in the position of the splitter vane could be clearly discerned. It is seen from the graph, figure (20), that the agreement with the theory developed, using Grove's empirical velocity correlation, is surprisingly good. A somewhat un

DISTRIBUTION OF HEAT TRANSFER COEFFICIENTS AROUND

CYLINDER FOR SOURCE WIDTH OF 9.5"

× EXPERIMENT, Re = 157 - 1445

□ THEORY, EQ.(2.5) & GROVE's [2a]
VELOCITY CORRELATION

GRAPH - FIGURE 20
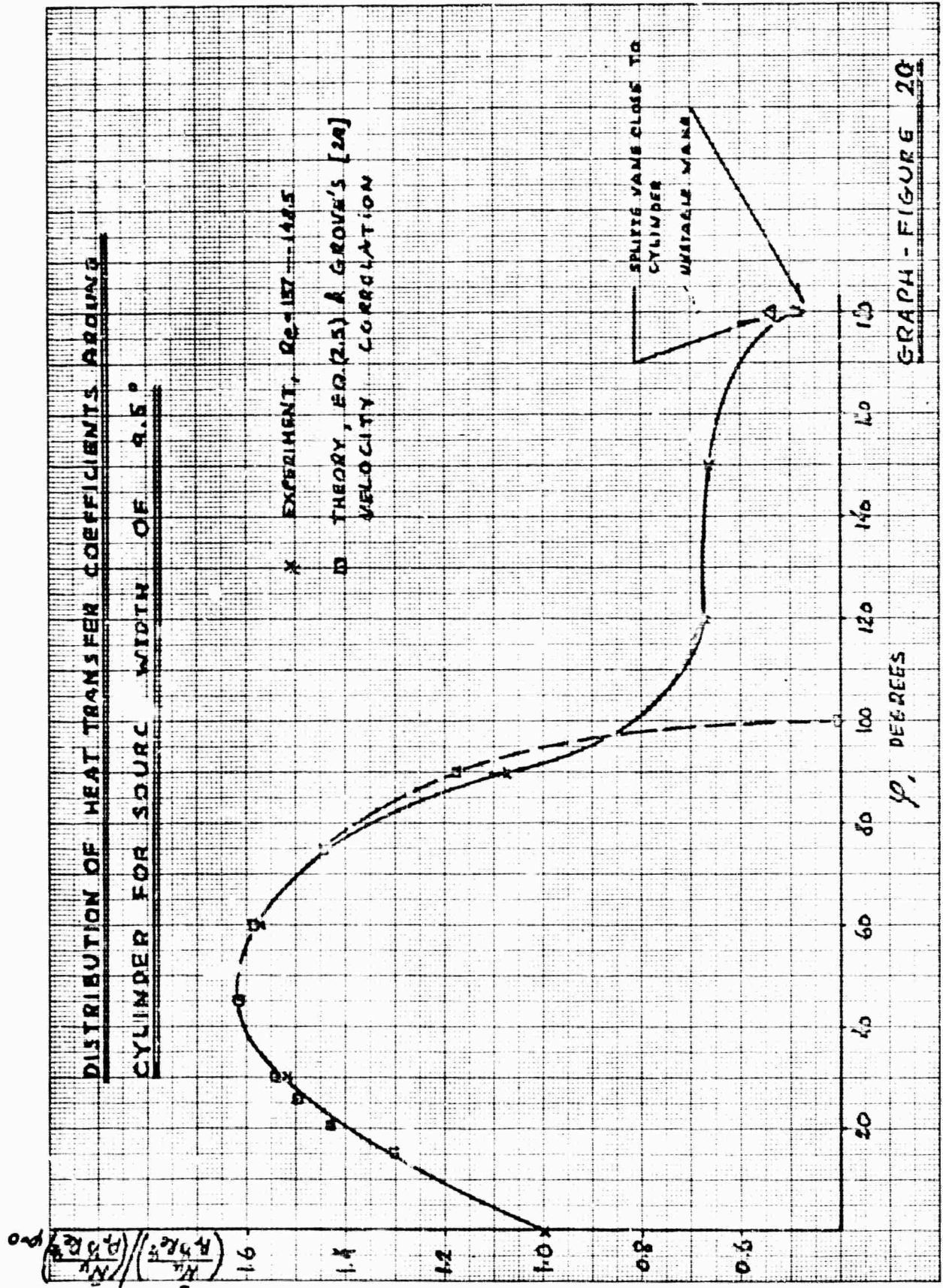
expected result is the notable variation of transfer coefficients as the the channel is traversed crosswise. This would point towards notable wall effects. The central thermocouple does indeed read temperatures which are considerably higher than those read by the two lateral ones. Doubtlessly, thermal conduction longitudinally along the strip could also have been of some importance, though it is believed that this latter effect cannot have been very important.

The cylinder with the strip type heat transfer surface was turned over to Mr. Snowden for further tests, which will be reported upon in [32].

List of References

[1] "Temperature and Velocity Profiles in the Compressible Laminar Boundary Layer with Arbitrary Distribution of Surface Temperature", by D. R. Chapman and N. W. Rubesin; J. Aero. Sc. 16, 1949, 547.

[2] "Heat Transfer to Constant Property Laminar Boundary Layer Flows with Power Function Free-Stream Velocity and Wall Temperature Variation", by S. Levy; J. Aero. Sc. 19, 1952, 341.

[3] "Contributions to the Theory of Heat Transfer Through a Laminar Boundary Layer", by M. J. Lighthill; Proc. Roy. Soc. A. 202, 1950, 359-377; also in "Recent Advances in Heat and Mass Transfer", J. P. Hartnett, editor, McGraw-Hill (New York 1961), 1-21.

[4] "On Heat Transfer in Laminar Boundary Layer Flows of Liquids Having a Very Small Prandtl Number", by G. W. Morgan, A. C. Pipkin, and V. H. Warner; J. Aero. Sc. 25, 1958, 173.

[5] "Heat Transfer to Fluids with Low Prandtl Number for Flow Across Plates and Cylinders of Various Cross-Section", by R. J. Grosh and R. D. Cess; Trans ASME 80, 1958, 667.

[6] "Details of Exact Low Prandtl Number Boundary Layer Solution for Forced and for Free Convection", by E. M. Sparrow and J. L. Gregg; NASA 2-57-59E, 1959.

[7] "On the Solution of the Convection Equation in Laminar Boundary-Layer Flows", by A. Acrivos; Chem. Engng. Sc. 17, 1962, 457-465.

[8] "Wärmeabgabe von geheizten Drähten und Rohren im Luftstrom", by R. Hilpert; VDI Forsch. 4, 1933, 215-224.

[9] "Local Nusselt Numbers for the Flow of Air Past Cylinders at Low Reynolds Numbers", by E. R. G. Eckert and E. Soehngen; Trans ASME 74, 1952, 343.

[10] "Boundary Layer Theory", by H. Schlichting, translated by J. Kestin; 4th ed., McGraw-Hill (New York, 1960); Chapter XIV.

[11] "Laminar Boundary Layers", L. Rosenhow, editor; Oxford University Press (London, 1963).

[12] "Fluid Dynamics and Heat Transfer", by J. G. Knudsen and D. L. Katz; McGraw-Hill (New York, 1958).

[13] "A Rapid Method for Estimating the Shear Stress and the Separation Point in Laminar Incompressible Boundary Layer Flows", by A. Acrivos; Reader's Forum, J. Aero. Space Sc. 27, 1960, 314-15.

[14] "An Experimental Investigation of the Steady, Separated Flow Past a Circular Cylinder", by A. S. Grove, A. Acrivos, H. Shair and E. E. Petersen, J. Fluid Mechs. 19, 1964, 60-80.

[15] "The Nature of the Steady, Separated Flow Past a Circular Cylinder at Large Reynolds Numbers", by A. Acrivos, A. S. Grove, and E. E. Petersen; submitted for publication to the J. Fluid Mechs., 1964.

[16] J. Lévêque; Annales des Mines 13, 1928, 201-381.

[17] "On the Rate of Heat Transfer in Laminar Boundary Layer Flows of Non-Newtonian Fluids Past a Horizontal Cylinder", by M. J. Shah; Ph. D. thesis, Dep. of Chem. Engng. University of California (Berkeley, 1961).

[18] J. A. Schnautz, Ph. D. thesis, Oregon State College (Cornwallis, 1958).

[19] "Physicochemical Hydrodynamics", by V. G. Levich; Prentice Hall (New York, 1962).

[20] "Elektrochemische Messung von Stoffübergangszahlen", by P. Grassmann, N. Ibl and J. Trüb; Chem. Ing. Tech. 33, 1961, 529-533.

[21] "Natural Convection Mass-Transfer Measurement on Spheres and Horizontal Cylinders by an Electrochemical Method", by G. Schütz; Int. J. Heat and Mass Transf. 6, 1963, 873-879.

[22] "Rates of Electrode Processes by the Rotating Disk Method", by D. Jahn and W. Vielstich; J. Electrochem. Soc. 109, 1962, 849-852.

[23] Personal communication, Dr. N. Ibl, 1964.

[24] International Critical Tables, 1st ed., McGraw-Hill (New York, 1928), III, 92, 106.

[25] "Natural Convection Mass Transfer at Vertical Electrodes under Turbulent Flow Conditions", by M. G. Fouad and N. Ibl; Electrochimica Acta 3, 1960, 233.

[26] "On the Development of Turbulent Wakes from Vortex Streets", by Anatole Roshko; NACA TN 2913, 1953, 77 pp.

[27] "On the Drag and Shedding Frequency of Two-dimensional Bluff Bodies", by Anatole Roshko; NACA TN 3169, 1954, 29 pp.

[28] "Theoretical and Experimental Investigations of Fluid Flow and Heat Transfer around a Cylinder in the Region of Low Reynolds Number and High Prandtl Number", by F. H. Shair; Ph. D. thesis, Univ. California (Berkeley, 1963).

[29] "An Investigation into the Nature of Steady Separated Flows at Large Reynolds Numbers, by A. S. Grove; Ph. D. thesis, Univ. California (Berkeley, 1963).

[30] Personal communication, A. Acrivos, 1964.

[31] "The Effect of Confining Walls on the Stability of the Steady Wake Behind a Circular Cylinder", by F.H. Shair, A.S. Grove, E.E. Petersen and A. Acrivos; J. Fluid Mechs. 17, 1963, 546-550.

[32] In preparation, D.D. Snowden.

[33] Stanford Computor Library Program No. 76 by J. Welsch.

[34] "Advanced Calculus for Applications", by F.B. Hildebrand;Prentice-Hall (Englewood Cliffs, 1963), 150 - 152.

[35] "Bestimmung von Diffusionskoeffizienten einiger Ionen in wässriger Lösung", by M. v. Steckelberg, M. Pilgram and V. Toome; Z. für Elektrochem. 57, 1953, 342-348.

[36] "Note on the Design and Construction of a Heat Transfer Test Cylinder for Constant Flux Wall Conditions", by Z. Rotem; Dep. Chem. Engng., Stanford Univ. (Stanford, 1964).

[37] "Solution of the Laminar Boundary Layer Energy Equation at High Prandtl Numbers", by A. Acrivos; Phys. of Fluids 3, 1960, .

Appendix I.

Expansion of u (x, y) near a flow boundary at which a no-slip condition applies.

At any solid boundary of a flow   the following conditions apply:

$$u_1 = v_1 = 0 \qquad \qquad \ldots (I\text{-}1)$$

where u_1 and v_1 are the dimensional velocities in the x_1 direction (parallel to the boundary) and the y_1 direction (perpendicular to the boundary) respectively. The momentum equation at the boundary thus degenerates to,

$$-\frac{\partial p}{\partial x_1} + \mu \left. \frac{\partial^2 u_1}{\partial y_1^2} \right|_{y_1 = 0} = 0 \qquad \qquad \ldots (I\text{-}2)$$

Assuming that u_1 is an analytic function of the ordinate y_1,

$$u_1(x_1, y_1) \Big|_{x = \text{constant}} = \delta(y_1)$$

then,

$$\delta(y_1) = \delta(0) + \delta'(0)\frac{y}{1!} + \delta''(0)\frac{y}{2!} + \ldots \qquad \ldots (I\text{-}3)$$

Now, from (I-1)

$$\delta(0) \equiv ; \text{ also.}$$

$$\delta'(0) = \partial u / \partial y \Big|_{y_1 = 0} = \tau(x_1, y_1)/\mu \Big|_{y_1 = 0} = \tau_0(x)/\mu$$

and from (I-2),

$$\delta''(0) = \frac{1}{\mu}\frac{\partial p}{\partial x_1}; \qquad \delta'''(0) = 0 \qquad \qquad \ldots (I\text{-}4)$$

We shall insert these results into the momentum equation so as to obtain the higher order terms. Integrating twice we find that the expansion for u_1 correct to the 5th order terms is,

$$u_1(x_1, y_1) = \frac{\tau_0}{\mu} y_1 + \frac{y_1^2}{\mu}\frac{dp}{dx} - \frac{y_1^3}{6\mu}\frac{d^2 \tau_0}{dx_1^2} + \frac{y_1^4}{24\mu}\left(\frac{\rho}{\mu^2}\tau_0\frac{d\tau_0}{dx_1} - \frac{d^3 p}{dy_1^3}\right)$$
$$+ \frac{y_1^5}{60\mu}\left(\frac{1}{2}\frac{d^4 \tau_0}{dx_1^4} + \frac{\rho}{\mu^2}\tau_0\frac{d^2 p}{dx_1^2} + \ldots \qquad \ldots (I\text{-}5)$$

If the energy equation is to be solved for fluids of very large Prandtl numbers, the expression for u_1 may be linearized, retaining only the first term of the expansion, as the thermal boundary layer is very thin compared to the momentum boundary layer. This is essentially the Lévêque assumption [16, 12].

Equation (I-5) may be rendered dimensionless, thus,

$$u(x,y) = \beta(x) Y + \frac{1}{2} Y^2 \frac{d\pi}{dx} - \frac{Y^3}{6 Re} \cdot \overset{O}{\overbrace{\frac{d^2\beta(x)}{dx^2}}} + \frac{1}{24} \beta \frac{d\beta}{dx} Y^4$$

$$- \frac{1}{24 Re} Y^4 \cdot \overset{O}{\overbrace{\frac{d^3\pi}{dx^3}}} + \ldots \qquad \ldots (I-6)$$

Appendix II

Calculation of the temperature of a metal strip containing distributed heat sources, cooled by convection of a high-Prandtl number fluid over its surface. Figure (II-1) illustrates the nomenclature used.
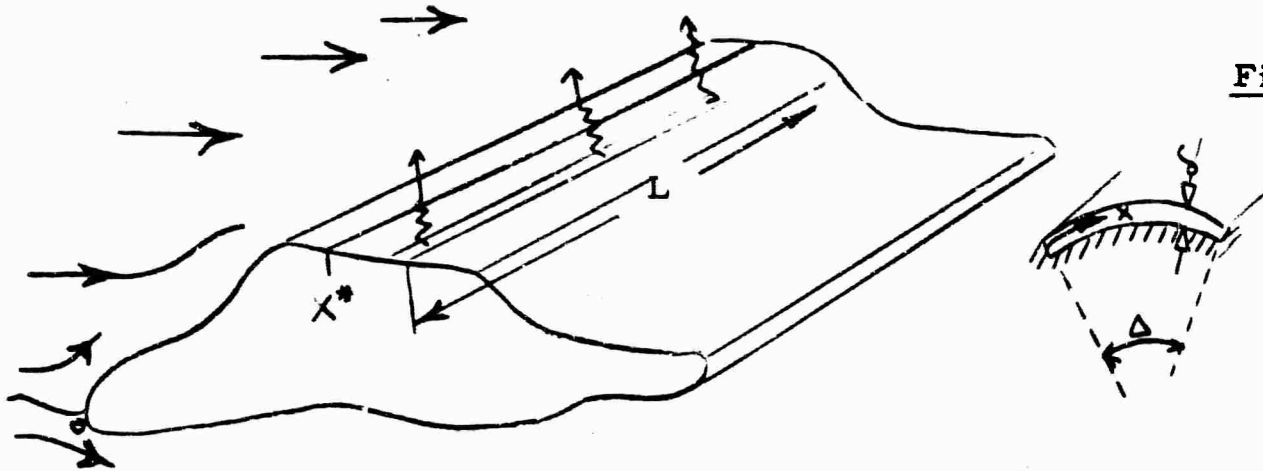
Figure 21

Curvature and thickness effects are neglected. The conduction equation for the heating strip then reduces to,

$$\frac{d}{dx}\left(K_s(\theta)\frac{d\theta}{dx}\right) + q_s'''(\theta) - \frac{H(x,\theta)}{\delta}\cdot\theta = 0 \qquad \ldots(II-1)$$

where θ is the excess temperature;

K_s is the conductivity of the solid wall material;

H is the surface convection coefficient and δ is strip thickness;

q_s''' is heat source strength per unit volume of material; for electrical heating,

$$q_s''' = C V^2/(\rho_e L^2) \qquad \ldots(II-2)$$

where V is the applied electrical potential difference over a strip of length l and electrical resistivity $\rho_e(\theta)$; C is a dimensional constant (equal to 0.24 if q''' is in cgs units, V in volts and ρ in ohms cm).

The appropriate boundary conditions are,

$$x = x^* \quad \text{and} \quad x = x^* + \Delta \Rightarrow \theta_x = 0 \qquad \ldots(II-3)$$

We shall now assume all physical properties to be independent of temperature. Equation (I-1) may be written in dimensionless form thus,

$$\frac{d^2\vartheta}{dy^2} - Bi\,\vartheta + 1 = 0 \qquad \ldots(II-4)$$

Here $\varphi = x/r$, with r a reference length; ϑ is a dimensionless temperature

$$\vartheta = \theta/M$$

where M is the source strength, $M = q_s''' \, r^2/K_s$, and Bi is a Biot number,
$Bi = \dfrac{H}{K_s} \times \dfrac{r^2}{\zeta}$. Further introducing the asymptotic value of the heat transfer
coefficient for large Pr numbers, equation (2.3); transforming the coördinates
as follows,

$$\mathcal{X} = \varphi/\Delta$$

$$\mathsf{T} = \frac{K \text{ fluid}}{K \text{ solid}} \frac{r}{\zeta} \cdot \frac{1}{T_{s_0} - T_\infty} \frac{Re^{1/2} Pr^{1/3}}{9^{1/3} \Gamma(\frac{4}{3})} \cdot \frac{\theta}{\sqrt[3]{\Delta}} \qquad \ldots (II-5)$$

and introducing a parameter,

$$\mathcal{E} = \frac{K \text{ solid}}{K \text{ fluid}} \frac{\zeta}{r^3} \frac{T_{so} - T_\infty}{q_s'''} \frac{9^{1/3} \Gamma(\frac{4}{3})}{Re^{1/2} Pr^{1/3}} \frac{1}{\Delta^{5/3}} \qquad \ldots (II-5a)$$

we finally obtain,

$$\mathcal{E} \, \mathsf{T}_{xx} \cdot \sqrt{\beta(\mathcal{X})} \int_0^{\mathcal{X}_1} \frac{d\,T_s\,(\mathcal{X})}{\left[\int_{\mathcal{X}}^{\mathcal{X}_1} \sqrt{\beta(\nu)} \, d\nu\right]^{1/3}} + 1 = 0 \qquad \ldots (II-6)$$

with boundary conditions $\mathsf{T}'(0) = 0$ and $\mathsf{T}'(1) = 0$.

For almost isothermal heating of a metal strip such as in the diagram figure I-1,
the numerical value of the parameter $\mathcal{E}$ is very large indeed. If we introduce
the additional simplification of replacing, over the strip width in the flow dir-
ection, $\beta(\mathcal{X})$ by its average value, then a regular perturbation solution of
equation (II-6) is readily obtained. This yields an expression for the tempera-
ture distribution at any location $\mathcal{X}$ in ascending powers of $\frac{1}{\mathcal{E}}$:

$$\mathsf{T} = \frac{2}{3}\left[\bar{\beta}(x)\right]^{1/3} + \frac{1}{\mathcal{E}}\left(\frac{3}{5}\mathcal{X}_1^{5/3} - \frac{1}{2}\mathcal{X}_1^2 + \frac{9}{40} - \frac{1}{7}\frac{[\Gamma(\frac{3}{3})]^2}{\Gamma(\frac{4}{3})}\right)$$

$$+ \frac{9}{2\mathcal{E}^2}\left\{\left[\bar{\beta}(x)\right]^{1/3}\mathcal{X}_1^{5/3}\left[\frac{9}{40}\left(\frac{\mathcal{X}_1^2}{11} - \frac{1}{5}\right) - \frac{1}{7}\frac{[\Gamma(\frac{3}{3})]^2}{\Gamma(\frac{4}{3})}\left(\frac{\mathcal{X}_1^{5/3}}{10} - \frac{1}{5}\right)\right] + C_4\right\}$$

$$+ 0\left|\frac{1}{\mathcal{E}^3}\right| \qquad \ldots (II-7)$$

The constant C_4 has to be determined from a heat balance calculation.
In the practical case of the heat transfer cylinder with a copper strip described
above the numerical value of the parameter $\mathcal{E}$ was about 21.

II. 2

We shall now consider the case of a metal strip which forms an <u>almost</u> <u>constant flux</u> surface: i.e. the parameter $\mathcal{E}$ is now very small. While in the previous case a passage to the limit $\mathcal{E}\to\infty$ did not decrease the order of the differential equation involved, and hence a regular perturbation scheme could be evolved, in the case to be now analyzed the limit $\mathcal{E}\to 0$ would decrease the order of the equation: we shall therefore expect to have to evolve a singular perturbation scheme. This is, however, not straightforward in the present case.

Considering the actual physical configuration, the importance of the second derivative in the equation (the conduction term) is significant only near the boundaries of the strip, where this term will have to insure the fulfillment of the boundary conditions. Over the rest of the strip a "core solution" will be operative and conduction will be unimportant.

Proceeding as in the case supra, our basic equation is still (II-4), however now with a very <u>large</u> value of Bi. Replacing H from equation (2. 12) we now get,

$$Bi = \frac{K \text{ fluid}}{K \text{ solid}} \; \frac{r}{\delta} \; 3^{1/3} \Gamma(\tfrac{4}{3}) \; Pr^{1/3} Re^{1/2} \left\{ \int_{x^*}^{x} \frac{dx}{[\gamma(x_1)-\gamma(x)]^{2/3}} \right\}^{-1} \qquad \ldots (II-8)$$

and finally,

$$T = \frac{K \text{ fluid}}{K \text{ solid}} \; \frac{r}{\delta} \; 3^{1/3} \Gamma(\tfrac{2}{3}) \; Pr^{1/3} Re^{1/2} \frac{\theta}{\Delta \cdot M} \qquad \ldots (II-9)$$

$$\mathcal{E} = \frac{K \text{ solid}}{K \text{ fluid}} \; \frac{\delta}{r} \; \frac{Re^{-1/2} Pr^{-1/3}}{3^{1/3} \Gamma(\tfrac{4}{3}) \Delta} \qquad \ldots (II-10)$$

$$\mathcal{E} T' - \frac{T}{\displaystyle\int_{0}^{x} \frac{dx}{[\gamma(x_1)-\gamma(x)]^{2/3}}} + 1 = 0 \qquad \ldots (II-11)$$

The use of eq. (2. 14) instead of (2. 12) in the development above is unfortunately not possible as it leads to an equation which is not easily soluble. Solution of (II-11)[*] therefore proceeds best numerically. This was carried out on the Stanford B5000 digital computer . The program makes use of the Fourth Order Adams-

[*] Using (2. 12) to evaluate the integral.

Bashforth Predictor - Corrector Method for the numerical integration [33], [*],
and results are given below and in figure (19), and table (I).

The equation to be solved is,

$$T'' - \frac{T}{x^{1/3}} + 1 = 0 \qquad \qquad \ldots (II-12)$$

with,

$$T = \frac{K_{fluid}}{K_{solid}} \cdot \frac{r}{\delta} \cdot \Gamma(\tfrac{2}{3}) \left[\frac{Pr.\bar{\beta}}{9.\Delta} \right]^{1/3} Re^{1/2} \cdot \frac{\Theta}{M} \qquad \qquad \ldots (II-13)$$

$$\mathcal{E} = \frac{K_{solid}}{K_{fluid}} \cdot \frac{\delta}{r} \cdot \frac{1}{\Gamma(\tfrac{2}{3})} \left[\frac{9}{\beta Pr \Delta^5} \right]^{1/3} Re^{-1/2} \qquad \qquad \ldots (II-14)$$

and boundary conditions,

$$T'(0) = T'(1) = 0 \qquad \qquad \ldots (II-15)$$

As explained above, the importance of the second derivative term in the equation
(II-12) will be felt in narrow "boundary layers" near $x = 0$ and $x = 1$. Near these
boundary points all terms in the equation should become of comparable order of
magnitude. This may be emphasized by introducing streched coördinates as
follows:

$$\hat{T} = \mathcal{E}^{1/5} T ; \qquad \qquad \bar{x} = \mathcal{E}^{3/5} x; \qquad \qquad \ldots (II-16)$$

The boundary $\bar{x} = 0$ coincides with $x = 0$ for any non-zero $\mathcal{E}$. We thus see
immediately that near that boundary $T \propto \mathcal{E}^{1/5}$ [+]. Table II below gives some
numerical data:

T A B L E   II

	0.20	0.15	0.10	0.05	0.001
$T_{(\mathcal{E}=0.20)}/T_0$ numerical integrtn.	1.00000	1.03737	1.09867	1.21640	1.95254
$(0.20/\mathcal{E})^{1/5}$	1.00000	1.0391	1.1488	1.3195	1.810

---

[*] The author is indebted to Mr. Ury Passy for help with the numerical analysis.

[+] This was pointed out to the author by Dr. A. Acrivos.

PROGRAM FOR NUMERICAL INTEGRATION

```
                    STANFORD B5000 ALGOL -- 7/23/64 VERSION        216/64
BEGIN COMMENT ROTEM ZEEV CONDUCTION EFFECT CALCULATIONS FOR THE CONSTANT
FLUX CASE FOR VARIOUS BIOT NUMBER VALUES BY ADAMS BASHFORTH INTEGRATION;
REAL ZETA,EPSI;INTEGER K,I;REAL ARRAY XPR,XFL[1:2],INITIAL1,FINAL2
[0:100];LABEL END1,END2,DOAGAIN;
FORMAT FMT1(////,"THE VALUE OF EPSILON IS NOW",X2,F5.3);
PROCEDURE FUNCT(NU,XPR,F);VALUE NU;REAL NU;REAL ARRAY XPR[*],F[*];
BEGIN F[1]+XPR[2];F[2]+(XPR[1]/NU*(1/3)-1)/EPSI;END FUNCT;
REAL ARRAY KFORADAMS[0:3,1:30], YINCFORADAMS[1:30]; COMMENT GOES
BEFORE ADAMS;
PROCEDURE  ADAMS(SIZE, HZERO, INITIAL, FINAL, PRINT, RELB, ABSB,
                 YINITIAL, YFINAL, FUNCT) ;
    VALUE SIZE, HZERO, INITIAL, FINAL, PRINT, RELB, ABSB ;
    INTEGER  SIZE ;  REAL  HZERO, INITIAL, FINAL, PRINT, RELB, ABSB ;
    REAL ARRAY  YINITIAL, YFINAL[1] ;
    PROCEDURE  FUNCT  ;
BEGIN COMMENT  ADAMS VERSION OF APRIL 1, 1964 ;



RETURN;  END ADAMS ;
FOR EPSI+5@-2 STEP 5@-2 UNTIL 0.3 DO BEGIN I+0;WRITE(FMT1,EPSI);
XPR[1]+5X@-1;XPR[2]+0;
INITIAL1[I]+XPR[1];K+0;ZETA+0.1;FOR I+1 STEP 1 UNTIL 100 DO BEGIN
DOAGAIN; ADAMS(2,0.01,@-10.1,ZETA,@-7,@-7,XPR,XFL,FUNCT);
IF ABS(XFL[2])> @-6 THEN BEGIN IF I=1 THEN BEGIN FINAL2[I-1]+XFL[2];
XPR[1]+INITIAL1[I]+INITIAL1[I-1]+@-4;GO TO END1;END ELSE BEGIN
FINAL2[I-1]+XFL[2];XPR[1]+INITIAL1[I]+INITIAL1[I-1]-(INITIAL1[I-1]
-INITIAL1[I-2])/(FINAL2[I-1]-FINAL2[I-2])XFINAL2[I-1];GO TO END1;END;
END;IF K=0 THEN BEGIN K+1;ZETA+0.05;GO TO DOAGAIN;END;IF K#0 THEN GO TO
END2;END1;END;END2;END;END.
```

RESULTS OF NUMERICAL
INTEGRATION OF EQUATION (II-12)
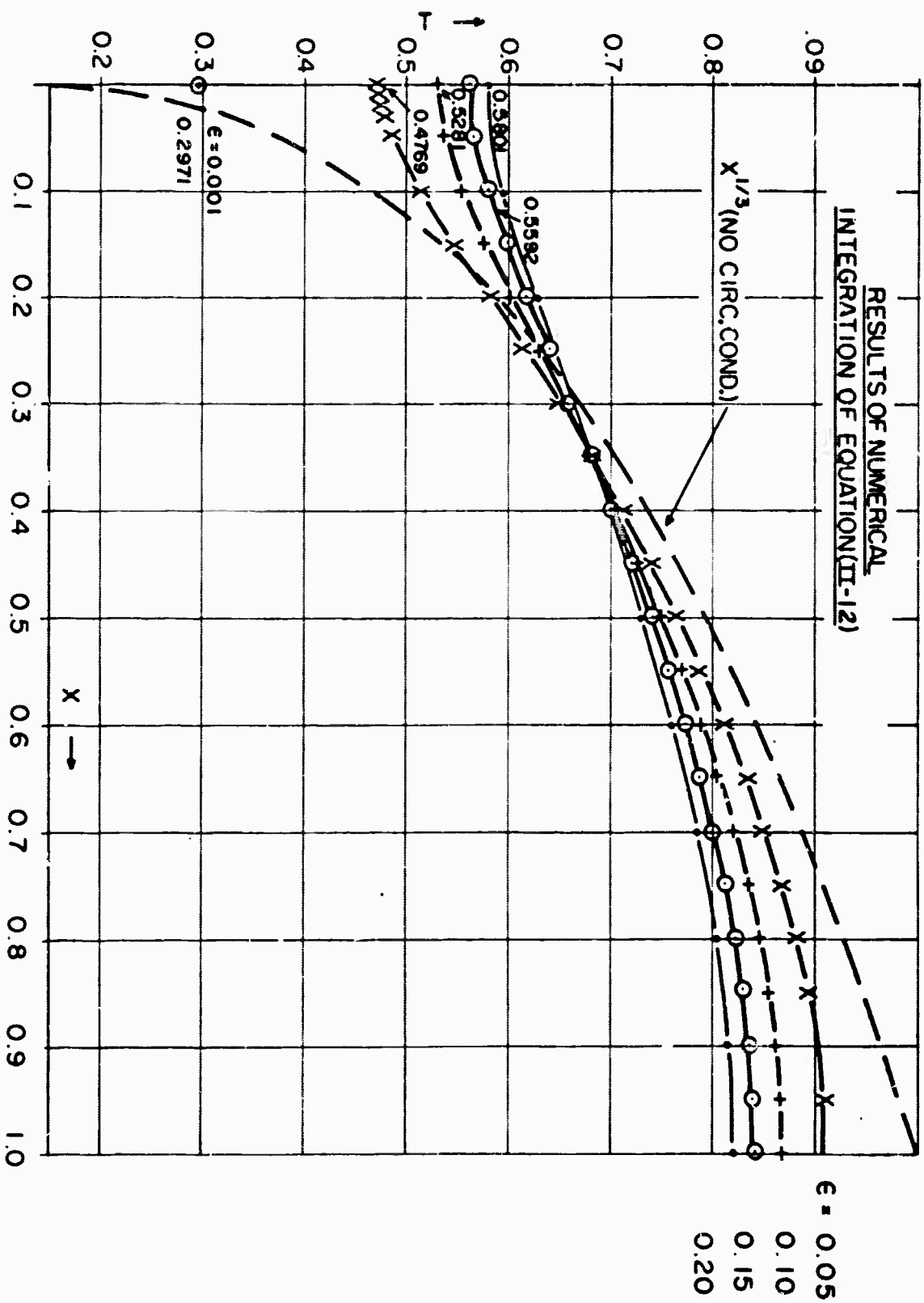
GRAPH FIGURE 22

TABLE   I :

EXAMPLE OF RESULTS OF NUMERICAL INTEGRATION FOR EPSILON = 0.05

```
                            T(X)              T'(X)
X = 1.000000000000-10
                4.768667365930-01    0.000000000000+00
     THE STEP SIZE IS NOW 3.725290298480-10
     THE STEP SIZE IS NOW 1.862645149230-10
     THE STEP SIZE IS NOW 3.725290298480-10
     THE STEP SIZE IS NOW 7.450580597000-10
     THE STEP SIZE IS NOW 1.490116119380-09
     THE STEP SIZE IS NOW 2.980232238770-09
     THE STEP SIZE IS NOW 5.960464477600-09
     THE STEP SIZE IS NOW 1.192092895510-08
     THE STEP SIZE IS NOW 2.384185791020-08
     THE STEP SIZE IS NOW 4.768371582030-08
     THE STEP SIZE IS NOW 9.536743164100-08
     THE STEP SIZE IS NOW 1.907348632810-07
     THE STEP SIZE IS NOW 3.814697265630-07
     THE STEP SIZE IS NOW 7.629394531300-07
     THE STEP SIZE IS NOW 1.525878906250-06
     THE STEP SIZE IS NOW 3.051757812510-06
     THE STEP SIZE IS NOW 6.103515625000-06
     THE STEP SIZE IS NOW 1.220703125000-05
     THE STEP SIZE IS NOW 2.441406250000-05
     THE STEP SIZE IS NOW 4.882812500010-05
     THE STEP SIZE IS NOW 9.765625000000-05
     THE STEP SIZE IS NOW 1.953125000000-04
     THE STEP SIZE IS NOW 3.906250000000-04
     THE STEP SIZE IS NOW 7.812500000000-04
     THE STEP SIZE IS NOW 1.562500000000-03
X = 5.000000010010-02
                4.864602642750-01    4.288474179670-01
     THE STEP SIZE IS NOW 3.125000000010-03
X = 1.000000001000-01
                5.135852275040-01    6.216237278400-01
X = 1.500000001000-01
                5.465376022770-01    6.836856259900-01
X = 2.000000000990-01
                5.810903480500-01    6.926547898700-01
     THE STEP SIZE IS NOW 6.250000000000-03
X = 2.500000000990-01
                6.153988956600-01    6.769169586900-01
X = 3.000000000970-01
                6.485871688220-01    6.492879350300-01
X = 3.500000000970-01
                6.802364310100-01    6.160857251100-01
X = 4.000000000960-01
                7.101568919100-01    5.805004510900-01
     THE STEP SIZE IS NOW 1.250000000000-02
X = 4.500000000960-01
                7.382729616300-01    5.440746512640-01
X = 5.000000000950-01
                7.645608703800-01    5.074217069080-01
X = 5.500000001000-01
```

```
                7.8901243547 00-01      4.7059533252 00-01
X = 6.00000000090 0-01
                8.1161246012 00-01      4.3328396380 80-01
X = 6.50000000090 0-01
                8.3232324 78 10 0-01     3.9491050996 40-01
     THE STEP SIZE IS NOW 2.50000000010-02
X = 7.00000000090 0-01
                8.5107262 983 00-01      3.5467728672 50-01
X = 7.50000000090 0-01
                8.6774331316 00-01      3.1157657808 70-01
X = 8.00000000090 0-01
                8.8216211317 00-01      2.6437761007 80-01
X = 8.50000000090 0-01
                8.9408816436 00-01      2.1159579900 70-01
X = 9.00000000090 0-01
                9.0319905526 00-01      1.5144553712 00-01
X = 9.50000000090 0-01
                9.0907430121 00-01      6.1777550286 00-02
X = 1.00000000000 +00
                9.1117526715 00-01      8.4310909187 00-07
```

Near the other boundary the investigation of the properties of the solution proceeds as follows: the complementary solution to (II-12) is,

$$T = \hat{x}^{1/2}\left[c_1 I_{3/5}(-\frac{6}{5}\hat{x}^{5/6}) + c_2 K_{3/5}(-\frac{6}{5}\hat{x}^{5/6}) \right] \qquad \ldots (II\text{-}17)$$

with $\hat{x} = x.\varepsilon^{-3/5}$; the value of the particular solution of the full equation is approximately unity at $x = 1$ (i.e. $\hat{x} \to \infty$). Now, as the function $I_{3/5}$ diverges as the argument increases without limit we must have $c_1 = 0$; also, an asymptotic expansion may be used for the function $K_{3/5}$.[*] The result is then easily derived that

$$1 - T \propto \varepsilon^{1/4}. \exp(-1/\sqrt{\varepsilon}) \qquad \ldots (II\text{-}18)$$

This agrees qualitatively with the results of the numerical integration.

Standard singular perturbation analysis would, of course, yield $\Delta T \propto \varepsilon^{1/2}$ using the standard stretching technique. From the numerical integration it appears however that for identical values of ε ratios, the ratio $\Delta T_1 / \Delta T_2$ depends on the absolute value of ε_1 also; of this the standard analysis gives no indication.

TABLE (III). Numerical Solution Near $x=1$.

ε	T	1 - T	$(1-T)/(1-T)_{(\varepsilon=0.05)}$	
0.05	0.911074	0.088926	1.000	
0.10	0.869471	0.130529	1.468	1.468
0.15	0.841093	0.158907	1.788	
0.20	0.82065	0.17935	2.018	1.374

---

[*] See c. f. [34], p. 150.

II.3

It is also possible to develop a simple integral approach for estimating the role of circumferential conduction.

Introduce the assumption of constant mean $\beta(x)$ into equation (2.11); then,

$$\theta_s(x_1) = q'' \frac{r}{K} 3^{2/3} \frac{Pr^{-1/3} Re_x^{-1/2}}{\Gamma(\frac{4}{3}) \beta^{1/3}} (x_1-x^*)^{1/3} \qquad \ldots (II-19)$$

whence

$$\frac{d\theta_s(x_1)}{dx_1} = q'' \frac{1}{K (3\beta)^{1/3}} \frac{Pr^{-1/3} Re_x^{-1/2}}{\Gamma(\frac{4}{3})} (x_1-x^*)^{-2/3} \qquad \ldots (II-20)$$

The circumferential flux per unit axial length of cylinder is then,

$$-K \text{ solid} \frac{\delta}{r} \frac{d\theta_s(x)}{dx_1} = q'' \delta \frac{K \text{ solid}}{K \text{ fluid}} \frac{Pr^{-1/3} Re_x^{-1/2}}{(3\beta)^{1/3} \Gamma(\frac{4}{3})} (x_1-x^*)^{-2/3} \qquad \ldots (II-21)$$

The radial flux per unit axial length of cylinder, for a strip of width $(x-x^*)$ is,

$$q'' r (x_1-x^*) \qquad \ldots (II-22)$$

Thus, a measure of the relative magnitude of circumferential to axial fluxes is obtained from (II-14) and (II-15):

$$\frac{1}{\overline{B}i} = \frac{1}{(3\beta)^{1/3} \Gamma(\frac{4}{3})} \frac{K \text{ solid}}{K \text{ fluid}} \frac{\delta}{r} \frac{Pr^{-1/3} Re_x^{1/2}}{(x_1-x^*)^{5/3}} \qquad \ldots (II-23)$$

i.e. the reciprocal of the Biot number is a direct estimate of the importance of circumferential flux compared to radial flux.

II.4

Finally, equation (II-11) gives the possibility of estimating the departure of an almost constant-flux surface from the ideal case when the parameter ε and the measured values of temperature are known.

Rewriting eq. (II-11) thus,

$$\varepsilon T'' - \frac{T}{\gamma(x)} + 1 = 0 \qquad \ldots (II-24)$$

$$\varepsilon \ll 1$$

leads to,

$$T = \gamma(x) + \varepsilon f(x) f''(x) + 0|\varepsilon^2| \qquad \ldots (II-25)$$

where $f(x)$ is obtained from the measured variation of T, and $f''(x)$ is then obtained through numerical differentiation of these values. Provided a sufficient

number of data points are taken, a first order correction can therefore be
obtained.   This is, however, liable to be a rather inaccurate procedure.   Now,
it is easily shown that,

$$Nu = 3^{1/3} \Gamma(\tfrac{2}{3}) \frac{Pr^{1/3} Re^{1/2}}{T} \qquad \ldots (II-26)$$

therefore

$$Nu = 3^{1/3} \Gamma(\tfrac{2}{3}) Pr^{1/3} Re^{1/2} \left[\frac{1}{f(x)} - \xi \frac{f''(x)}{f(x)} - 0|\xi^2| \right] \qquad \ldots (II-27)$$

Appendix III

Physical constants of electrolytic solution

There are wide discrepancies between values of the physical prop-
erties of our electrolytic test solution, as found by various investigators.
We were therefore prompted to compare these values in figures (21) through
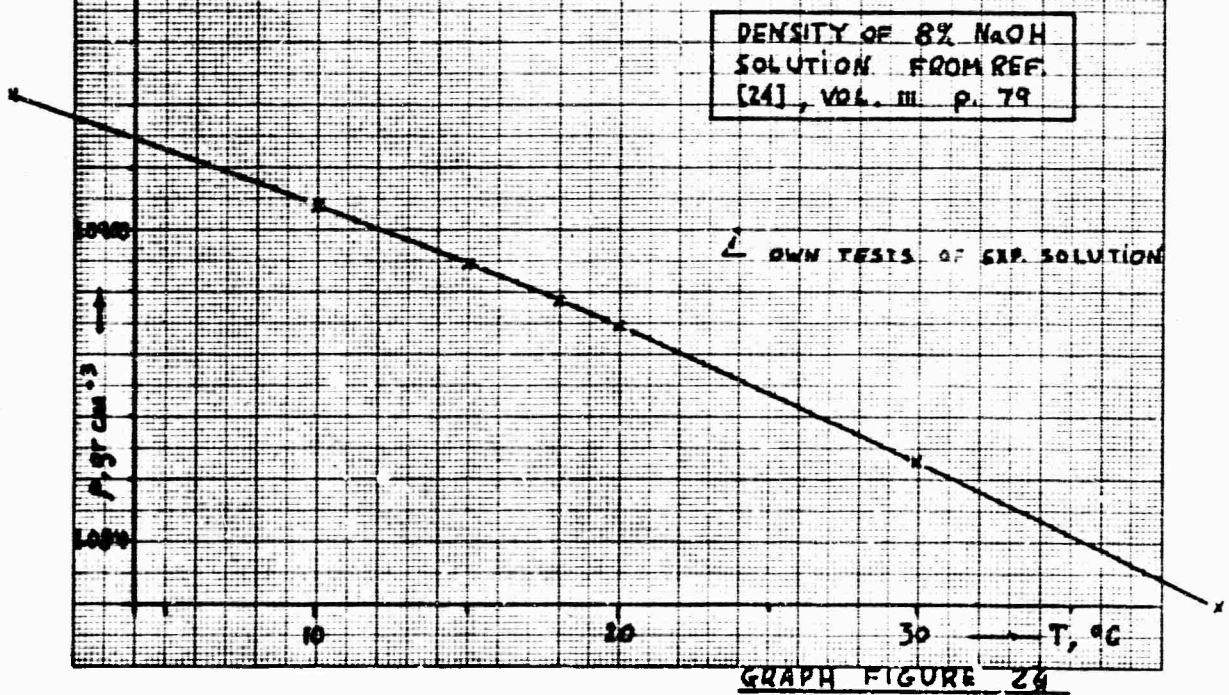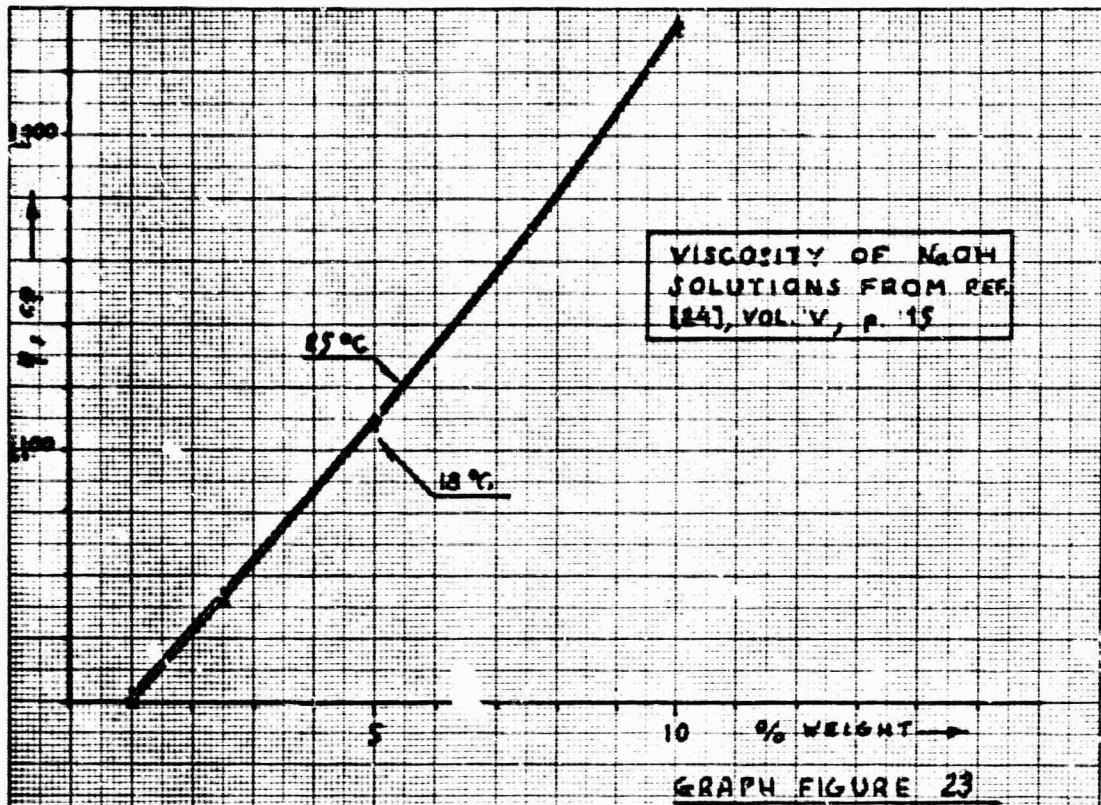(24).

It appears from an examination of figure (24) that both the composition
and concentration of supporting electrolyte seem to have a notable influence
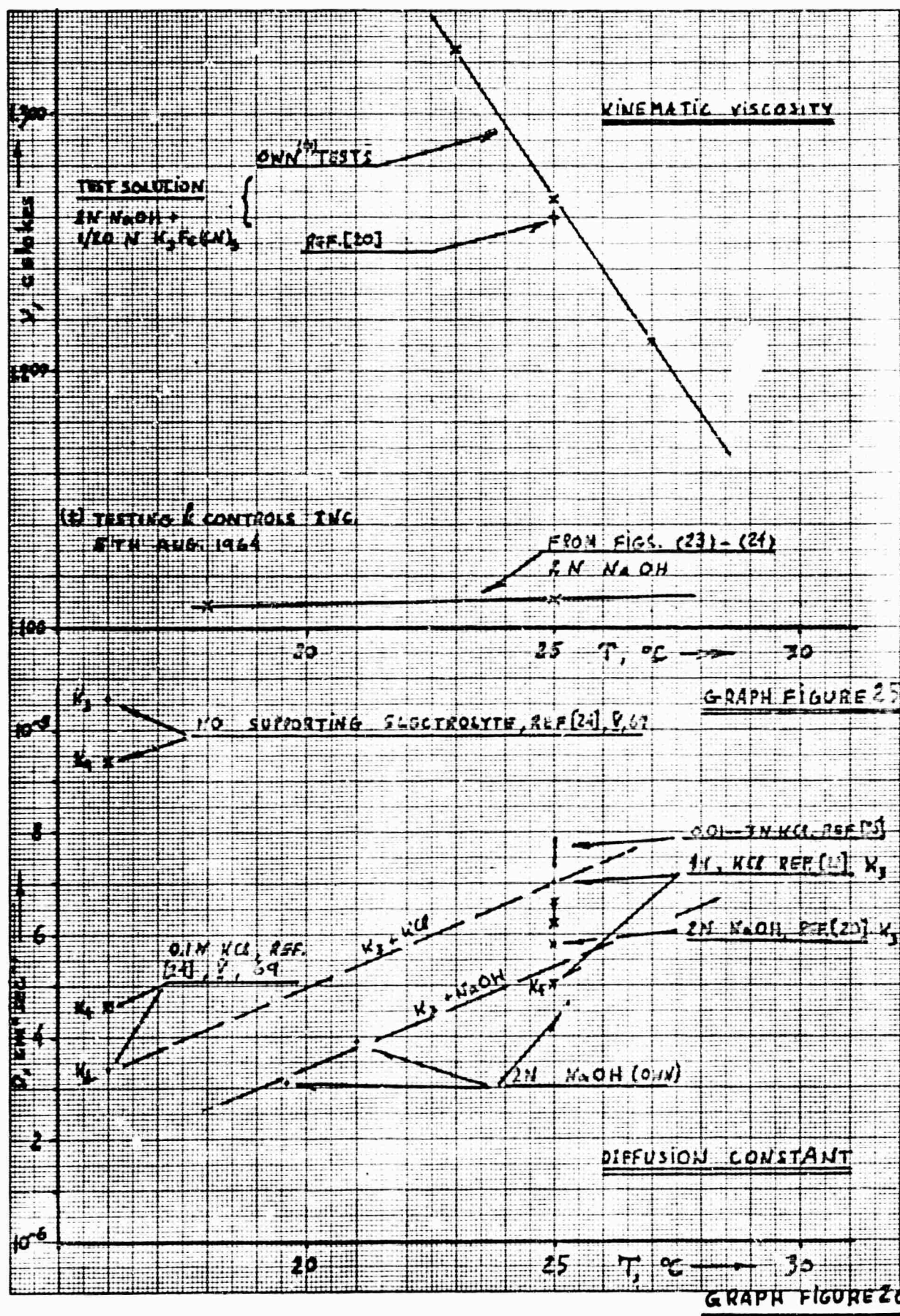on D, as well as the manner of testing.

The one systematice trend discernible seems to be the decrease in D
as supporting electrolyte is added. An unexpected feature is the fact that
$\mathcal{D}(K_4Fe(CN)_6)/\mathcal{D}(K_3Fe(CN)_6)$ can be either larger or smaller than unity,
depending on the temperature and on the concentration of supporting electro-
lyte. It also appears from [35] that diffusion coefficients found using KCl
as a supporting electrolyte are somewhat higher than those measured
with NaOH as supporting electrolyte.

Appendix IV

Data reduction of heat transfer experiments

For data reduction the Algol program of ref. [36] was used: this program
includes a correction taking into account the dependence of fluid viscosity on
temperature based on [37]. The sole modification introduced into the program
was a correction for the dependence of the electrical resistivity of the copper
heating strip on temperature. A printout of the program is given on page 60.

VISCOSITY OF NaOH
SOLUTIONS FROM REF.
[24], VOL. V, p. 15

GRAPH FIGURE 23

DENSITY OF 8% NaOH
SOLUTION FROM REF.
[24], VOL. III p. 79

∠ OWN TESIS OF EXP. SOLUTION

GRAPH FIGURE 24

KINEMATIC VISCOSITY

GRAPH FIGURE 25

DIFFUSION CONSTANT

GRAPH FIGURE 26

```
MUS[0]← 1.7800-(9.4757961-(6.0650639+(5.2299281-(5665.288-(245.582942
        -3.7946549×TH[0])×TH[0])×TH[0]×1.0P-4)×TH[0])×TH[0]×1.0P-2)
        ×TH[0]×1.0P-2)
PRS[0]←241.9048×CP[0]×MUS[0]/KTH[0])
PRS3[0]←PRS[0]↑(1/3))
FACTOR[0]←NU[0]/PRS3[0])
GFACTOR[0]←(1-(1-MUS[0]/MU[J])×0.095576)×FACTOR[0])
END)
WRITE(FMT12,FOR 0←1 STEP 1 UNTIL P DO TS[0]))
WRITE(FMT13,FOR 0←1 STEP 1 UNTIL P DO CP[0]))
WRITE(FMT14,FOR 0←1 STEP 1 UNTIL P DO KTH[0]))
WRITE(FMT15,FOR 0←1 STEP 1 UNTIL P DO NU[0]))
WRITE(FMT16,FOR 0←1 STEP 1 UNTIL P DO PRS[0]))
WRITE(FMT17,FOR 0←1 STEP 1 UNTIL P DO PRS3[0]))
WRITE(FMT18,FOR 0←1 STEP 1 UNTIL P DO FACTOR[0]))
WRITE(FMT19,FOR 0←1 STEP 1 UNTIL P DO GFACTOR[0]))
WRITE(FMT24))
END)
WRITE(FMT23,K))
GO TO LEOF1)
MIKAN1:WRITE(FMT9)) GO TO LEOF)MIKAN2:WRITE(FMT10))GO TO LEOF)
MIKAN3:WRITE(FMT20)) GO TO LEOF)MIKAN4:WRITE(FMT22))GO TO LEOF)
LEOF1:END)END)
LEOF:END.
```

```
?30
$JOB  T221  ALGOL 2     1200  ROTEM,DR ZEEV      293   NU STRIP CYLINDER
BEGIN COMMENT  ROTEM ZEEV  CALCULATION OF NU FOR STRIP CYLINDER;
INTEGER I,J,K,L1,L2,L3,L4,M,N,O,P,Q;
INTEGER ARRAY OMEGA[1:50];
REAL ARRAY Y,MJ,TBULK,UONE,RO,REYN,REHALF,VOLTAGE,THETA[1:50],
TS,KTH,CP,NU,PRS,PRS3,MUS,FACTOR,GFACTOR,TH,RESCOR[1:200];
LABEL START,MIKAN1,MIKAN2,MIKAN3,MIKAN4,LEOF,LEOF1;
FORMAT FMT1(///,X15,"RESULTS OF RUN",X2,I4,X3,"ARE AS FOLLOWS",//);
FORMAT FMT2("OMEGA=",X4,1F10.3),FMT3("TBULK=",X4,1F10.3),
FMT4("U1=",X7,1F10.3),FMT5("RO=",X9,1F9.4),
FMT6("MU(POISES)=",X3,1F8.5),FMT7("RE=",X7,F10.3),
FMT8("REHALF=",X3,1F10.3),
FMT9("NUMBER OF DATA POINTS OF TBULK # NUMBER OF DATA POINTS OF OMEGA"),
FMT10("NUMBER DATA POINTS VOLTS # THAT FOR OMEGA"),
FMT11("VOLTAGE=",X6,8F8.5),
FMT12("TS=",X8,8F9.3,X2),FMT13("CP=",X8,8F9.3,X2),
FMT14("K=",X10,8F9.4,X1),FMT15("NU=",X8,8F9.3,X2),
FMT16("PRS=",X7,8F9.3,X2),FMT17("PR1/3=",X5,8F9.3,X2),
FMT18("NU/(PR1/3)=",8F9.3,X2),FMT19("GNU/PR1/3=",X1,8F9.3,X2,//),
FMT20("NO CARD FOR M OR L1>20 OR L2>20 OR NO NUMB SWITCH POS"),
FMT21("L1=",I4),FMT22("OMEGA OR TBULK DATUM HAS VALUE ZERO"),
FMT23(/,X15,"END OF RUN",X1,I4),FMT24(//);
START:BEGIN READ (M);
IF M=0 THEN GO TO MIKAN3; IF M >12 THEN GO TO MIKAN3;
FOR N+1 STEP 1 UNTIL M DO BEGIN
READ(K,L1,FOR I+1 STEP 1 UNTIL L1 DO OMEGA[I]);
READ(L2,FOR I+1 STEP 1 UNTIL L2 DO TBULK[I]);
READ(L3,FOR I+1 STEP 1 UNTIL L3 DO VOLTAGE[I]);
IF  L1 # L2 THEN GO TO MIKAN1;IF L1>20 THEN GO TO MIKAN3;
FOR I+1 STEP 1 UNTIL L1 DO BEGIN
IF L3 # L1 THEN GO TO MIKAN2;
IF OMEGA[I]=0 THEN GO TO MIKAN4;IF TBULK[I]=0 THEN GO TO MIKAN4;END;
WRITE(FMT1,K); WRITE(FMT21,L1);
FOR J+1 STEP 1 UNTIL L1 DO  BEGIN
Y[J]+(OMEGA[J]+3×@-6)/25.773;
THETA[J]+TBULK[J]-20.00;
MU[J]+1.7800-(9.4757961-(6.0650639+(5.2299281-(5665.288-(245.582942
     -3.7946549×THETA[J])×THETA[J])×THETA[J]×1.0@-4)×THETA[J])×
     THETA[J]×1.0@-2)×THETA[J]×1.0@-2;
UONE[J]+12.25×SQRT(Y[J]/MJ[J]);
RO[J]+1.048330-((0.030225×TBULK[J]+4.306)×1.0@-6)×TBULK[J];
REYN[J]+1.905×UONE[J]×RO[J]/MU[J];
REHALF[J]+SQRT(REYN[J]);
WRITE(FMT2,OMEGA[J]);WRITE(FMT3,TBULK[J]);WRITE(FMT4,UONE[J]);
WRITE(FMT5,RO[J]);WRITE(FMT6,MU[J]);WRITE(FMT7,REYN[J]);
WRITE(FMT8,REHALF[J]);WRITE(FMT11,VOLTAGE[J]);
READ(P,FOR Q+1 STEP 1 UNTIL P DO TS[Q]);
IF P>20 THEN GO TO  MIKAN3;
FOR Q+1 STEP 1 UNTIL P DO BEGIN
CP[Q]+0.430+8.009@-4×(TS[Q]-10);
KTH[Q]+(9.262-6@-4×(TS[Q]-10))×1.0@-2;
RESCOR[Q] +1+(3.93@-3)×(TS[Q]-23.1);
NU[Q]+6.69163572@4×VOLTAGE[J]+2/((TS[Q]-TBULK[J])×RESCOR[Q]);
TH[Q]+TS[Q]-20.00;
```